

THE LUMINOSITY FUNCTION AT $z \sim 8$ FROM 97 Y-BAND DROPOUTS: INFERENCES ABOUT REIONIZATION

KASPER B. SCHMIDT¹, TOMMASO TREU¹, MICHELE TRENTI², LARRY D. BRADLEY³, BRANDON C. KELLY¹, PASCAL A. OESCH⁴, BENNE W. HOLWERDA⁵, J. MICHAEL SHULL⁶, AND MASSIMO STIAVELLI³

¹ Department of Physics, University of California, Santa Barbara, CA, 93106-9530, USA

² Kavli Institute for Cosmology and Institute of Astronomy, University of Cambridge, Madingley Road, Cambridge, CB3 0HA, United Kingdom

³ Space Telescope Science Institute, 3700 San Martin Drive, Baltimore, MD, 21218, USA

⁴ UCO/Lick Observatory, University of California, Santa Cruz, CA, 95064, USA

⁵ Leiden Observatory, Leiden University, NL-2300 RA Leiden, Netherlands and

⁶ CASA, Department of Astrophysical and Planetary Science, University of Colorado, Center for Astrophysics and Space Astronomy, 389-UCB, Boulder, CO 80309, USA

Draft version March 26, 2014

ABSTRACT

We present the largest search to date for Y-band dropout galaxies ($z \sim 8$ Lyman break galaxies, LBGs) based on 350 arcmin² of HST observations in the V-, Y-, J- and H-bands from the Brightest of Reionizing Galaxies (BoRG) survey. In addition to previously published data, the BoRG13 dataset presented here includes approximately 50 arcmin² of new data and deeper observations of two previous BoRG pointings, from which we present 9 new $z \sim 8$ LBG candidates, bringing the total number of BoRG Y-band dropouts to 38 with $25.5 \leq m_J \leq 27.6$ (AB system). We introduce a new Bayesian formalism for estimating the galaxy luminosity function, which does not require binning (and thus smearing) of the data and includes a likelihood based on the formally correct binomial distribution as opposed to the often used approximate Poisson distribution. We demonstrate the utility of the new method on a sample of 97 Y-band dropouts that combines the bright BoRG galaxies with the fainter sources published in Bouwens et al. (2011) from the Hubble Ultra Deep Field (HUDF) and Early Release Science (ERS) programs. We show that the $z \sim 8$ luminosity function is well described by a Schechter function over its full dynamic range with a characteristic magnitude $M^* = -20.15^{+0.29}_{-0.38}$, a faint-end slope of $\alpha = -1.87^{+0.26}_{-0.26}$, and a number density of $\log_{10} \phi^* [\text{Mpc}^{-3}] = -3.24^{+0.25}_{-0.24}$. Integrated down to $M = -17.7$ this luminosity function yields a luminosity density, $\log_{10} \epsilon [\text{erg/s/Hz/Mpc}^3] = 25.52^{+0.05}_{-0.05}$. Our luminosity function analysis is consistent with previously published determinations within 1σ . The error analysis suggests that uncertainties on the faint-end slope are still too large to draw firm conclusion about its evolution with redshift. We use our statistical framework to discuss the implication of our study for the physics of reionization. By assuming theoretically motivated priors on the clumping factor and the photon escape fraction we show that the UV luminosity density from galaxy samples down to $M = -17.7$ can ionize only 10-50% of the neutral hydrogen at $z \sim 8$. Full reionization would require extending the luminosity function down to $M = -15$. The data are consistent with a substantial fraction of neutral hydrogen at $z > 7$, in agreement with recent suggestions based on deep spectroscopy of redshift 8 LBGs.

Subject headings: cosmology: observations — galaxies: evolution — galaxies: formation — galaxies: high-redshift

1. INTRODUCTION

Characterizing the epoch of reionization, i.e., the epoch at which the first stars and galaxies in the Universe reionized the vast majority of the neutral hydrogen, is a key outstanding issue in the continued effort to map the formation and early evolution of galaxies. For almost four years, since the installment of the Wide Field Camera 3 (WFC3) onboard the Hubble Space Telescope (HST), the frontier of this knowledge has been pushed further and further back towards the dawn of cosmic reionization.

At present, several hundred high redshift galaxy candidates have been found at redshift $z \sim 6$ (e.g., Stark et al. 2010; Bouwens et al. 2007, 2012; Ouchi et al. 2010; Bradley et al. 2013), and with the improved near-IR efficiency of WFC3 the search for candidates has been

pushed to $z \gtrsim 8$ using the Lyman Break technique. In particular the Hubble Ultra Deep field efforts in 2009 (Oesch et al. 2010b,c; Lorenzoni et al. 2011; Bouwens et al. 2010, 2011; McLure et al. 2010) and 2012 (Koeke-moer et al. 2012; Ellis et al. 2012; Dunlop et al. 2012b; Schenker et al. 2013; McLure et al. 2013; Ono et al. 2012a; Oesch et al. 2013; Illingworth et al. 2013) have revealed the faintest samples of galaxy candidates at $z \gtrsim 8$. Simultaneously larger area observations are targeting brighter and rarer candidates, either in legacy fields, such as GOODS/CANDELS (Grogin et al. 2011; Koekemoer et al. 2011), or in pure-parallel random pointings, like those of our *Brightest of Reionizing Galaxies Survey*¹ (hereafter BoRG, Trenti et al. 2011, 2012b; Bradley et al. 2012).

kschmidt@physics.ucsb.edu

¹ <https://wolf359.colorado.edu>

Our ongoing BoRG survey has two key goals. The first goal is to provide bright targets that can potentially yield spectroscopic confirmation of $z \sim 8$ galaxies by follow-up observations (Treu et al. 2012, 2013). In fact, while $z \sim 6$ dropout samples have extensive spectroscopic redshifts, (e.g., Vanzella et al. 2009; Stark et al. 2010, 2013), only a handful of $z \gtrsim 7$ galaxies (e.g., Ono et al. 2012b) have currently confirmed redshifts with the highest being at $z = 7.5$ (Finkelstein et al. 2013). So far no Y-band dropout at $z \sim 8$ has been spectroscopically confirmed. Only upper limits on Ly α flux have been provided to date (Caruana et al. 2012, 2013; Capak et al. 2013; Treu et al. 2013; Faisst et al. 2014) and those leave open the interpretation of whether the photometric selection technique breaks down at $z \gtrsim 7$ (which would be surprising given the small change in magnitudes and filters) versus the more interesting physical explanation of an increase in the intergalactic medium (IGM) optical depth to Ly α arising from a higher neutral hydrogen fraction at $z \sim 8$ (Treu et al. 2013) with respect to redshift 7 (Fontana et al. 2010) and 6 (Stark et al. 2010, 2013).

The second goal of the BoRG survey is to improve the determination of the $z \sim 8$ luminosity function, by identifying rare and bright dropouts to extend the dynamic range of observations in smaller area deep fields, which are dominated by fainter sources. An accurate measure of the luminosity function is necessary not only to study how galaxies evolve across time, but also to quantify the photon budget available for hydrogen ionization (Trenti et al. 2010; Zaroubi 2013; Dunlop 2013). At lower redshift, it is well established (Bouwens et al. 2007) that the luminosity function is accurately described by a Schechter function (Schechter 1976) so it is natural to expect a similar form at higher redshift. However, data covering a wide dynamic range are needed to establish that this is indeed the case, and to resolve the degeneracy between the Schechter function parameters in the luminosity function fit (Bradley et al. 2012; Oesch et al. 2012).

In this paper we have two goals. The first is to present the complete sample of Y-band dropouts from the BoRG cycle-19 data, and to use these in combination with the literature to determine the galaxy luminosity function at $z \sim 8$. The second goal is to study the consequences for cosmic reionization the inferred luminosity function has. To determine the luminosity function we develop and implement a rigorous statistical Bayesian method to infer the posterior distribution function of the parameters of the luminosity function from the data. The method supersedes those commonly adopted in this field (e.g. Bradley et al. 2012; McLure et al. 2013; Schenker et al. 2013; Oesch et al. 2012) in several ways: the data are not binned, thus avoiding smearing the luminosity function (Trenti & Stiavelli 2008); the flux uncertainties are correctly taken into account; the counts are modeled using the formally correct binomial distribution (Kelly et al. 2008), instead of the Poisson approximation; the full posterior probability distribution function is computed using Markov Chain Monte Carlo methods instead of relying on maximum likelihood estimators based on the asymptotic covariance matrix from the observed Fisher information for uncertainties. By applying this framework to a large sample of $z \sim 8$ galaxies, consisting of $N = 97$ objects both bright (from BoRG) and faint (from the Hubble

UDF/ERS fields), we show that the credible intervals include previous best-fit estimates. By treating the problem in a self-consistent statistical manner we carry out an inference about reionization by combining the inferred observational uncertainties with various theoretical priors.

The paper is organized as follows. We start by briefly describing the BoRG survey in Section 2. The current sample of Y-band dropouts containing 9 new and 2 improved $z \sim 8$ galaxy candidates (BoRG13) with respect to those previously published by our team (BoRG09; BoRG12 Trenti et al. 2011; Bradley et al. 2012) is described in Section 3. Two Appendixes (A and B) take advantage of the follow-up observations of one field and of the large number of BoRG pointings to characterize and discuss the statistics of detections and contaminants in dropout searches. In Section 4 we apply our inference of the Schechter luminosity function parameters using our rigorous Bayesian framework, discussed in detail in Appendix C. The results are presented and discussed in the context of cosmic reionization in Section 5. A brief summary is given in Section 6.

All magnitudes are AB magnitudes and a standard concordance cosmology with $\Omega_m = 0.3$, $\Omega_\Lambda = 0.7$, and $h = 0.7$ is assumed.

2. THE BORG SURVEY

The $z \sim 8$ galaxy candidates from the latest data obtained as part of the BoRG survey are described briefly below. We refer the reader to Trenti et al. (2011) and Bradley et al. (2012) for a more in-depth description of the survey.

The BoRG survey is a pure-parallel WFC3 imaging HST program. As of April 2013 the survey has obtained ~ 350 arcmin² of visual and near-infrared HST photometry over 71 fields randomly located in the sky. The pure-parallel nature of the survey implies that the survey area is divided into 71 independent lines of sight on the sky, reducing sample (or cosmic) variance below the level of statistical noise (Trenti & Stiavelli 2008; Bradley et al. 2012). 53 out of the 71 fields represent the core of the BoRG survey and have been observed in the four WFC3/HST filters F606W, F098M, F125W, and F160W. This was primarily done as part of programs GO/PAR 11700 and GO/PAR 12572 (PI: Trenti) complemented by a small number of COS-GTO coordinated parallels. One of these 53 fields furthermore has data in F105W from a recent follow-up campaign (described in Appendix A). The core of BoRG is complemented by other archival data consisting of 8 fields from GO/PAR 11702 (PI: Yan, Yan et al. 2011) and 10 COS-GTO fields, where instead of the F606W-band the F600LP-band was used. For a discussion of the benefits of using F606W, as in the BoRG core, instead of F600LP see Bradley et al. (2012).

In this work we will refer to F606W, F098M, F125W, and F160W as V-, Y-, J-, and H-band observations unless mentioned otherwise. Note that the data added in BoRG13 only has F606W V-band observations as opposed to BoRG09 and BoRG12 which also contained F600LP V-band data.

3. Y-BAND DROPOUT SAMPLE

The dropout technique (Steidel et al. 1996, 2000; Madau et al. 1996) was applied to the BoRG data to

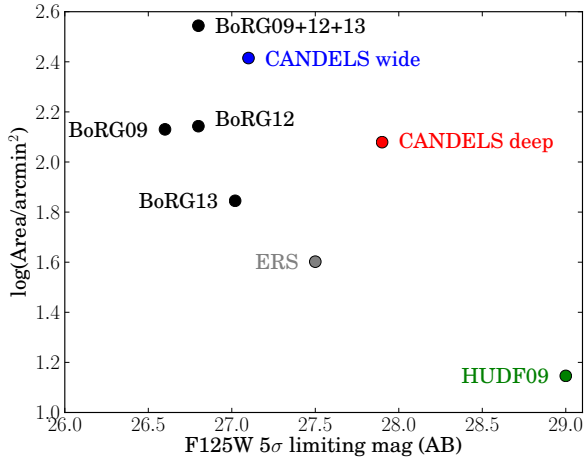


FIG. 1.— The area and depth of surveys where $z \sim 8$ Lyman Break Galaxy (LBG) dropout selection is currently possible. It is clear that BoRG is by far the largest area with the needed band coverage (VYJH). The CANDELS wide area for instance has Y-band coverage in approximately 260 arcmin². The HUDF and ERS fields were used to obtain the 59 $z \sim 8$ LBGs selected by Bouwens et al. (2011) used in the present study at the faint end of the luminosity function.

identify $z \sim 8$ galaxy candidates as detailed in Section 3.2

The first fields of the BoRG survey (referred to as BoRG09 and BoRG12) were analyzed by Trenti et al. (2011, 29 fields) and Bradley et al. (2012, 29+30=59). Based on this data, Bradley et al. (2012) presented a sample of 33 Lyman break galaxy (LBG) candidates at $z \sim 8$ and estimated the corresponding high-redshift luminosity function.

In this work we augment this sample by analyzing 13 additional fields, taken in HST Cycle 19 (GO/PAR 12572, PI: Trenti). Note that the field BoRG_1510+1115 also appeared in the study by Bradley et al. (2012) based on partial data. This field is therefore included in the present analysis and supersedes the previous release. Results of the analysis of the 13 new fields are presented in the next Section 3.1. We also present an updated analysis of BoRG_1437+5043 based on deeper and wider-field observations obtained in November 2012 (GO 12905, PI: Trenti). We describe these observations in Appendix A.

3.1. The Latest Survey Extension: BoRG13

The 13 new Cycle 19 BoRG fields are summarized in Table 1 together with the follow-up in BoRG_1437+5043. Together with Table 1 and Table 2 of Bradley et al. (2012) this summarizes the current status of BoRG09, BoRG12, and BoRG13. This brings the total J-band area of the BoRG survey to ~ 350 arcmin². This makes BoRG the largest existing area which can be searched for Y-band dropouts. In comparison, the CANDELS (Koekemoer et al. 2011; Grogin et al. 2011) survey has Y-band coverage of approximately 260 arcmin² (wide) and 120 arcmin² (deep). Furthermore the depth reached by BoRG (J and H ~ 26) at 5σ has not been achieved from the ground over large areas. The depth and area of the BoRG campaigns are compared with those achieved by other $z \sim 8$ surveys in Figure 1.

As noted in above and shown in Bradley et al. (2012) the effect of large scale structures, i.e. cosmic variance, is

less important than the statistical noise for the BoRG12 sample. Extending BoRG12 by the 13 new randomly pointed fields of BoRG13 makes cosmic variance even more negligible.

The BoRG13 fields were reduced using publicly available code. First, the cosmic rays were removed in each exposure using the Laplacian cosmic ray detection developed by van Dokkum (2001). The individual exposures in each filter were then combined using *AstroDrizzle* (the replacement of *MultiDrizzle* as of June 2012 Koekemoer et al. 2003). The images were drizzled to a final pixel scale of 0''.08/pixel using a ‘pixfrac’ of 0.75 as in our previous analyses. The correlated noise introduced by this drizzling (e.g., Casertano et al. 2000) is explicitly corrected for by normalizing the r.m.s. maps by the empirical noise as described by Trenti et al. (2011). The 5σ limiting magnitudes ($r = 0''.32$) and exposure times obtained in each field are quoted in Table 1.

Having created the reduced science images and r.m.s. maps we used *SExtractor* (Bertin & Arnouts 1996) in dual-image mode with the J-band image as detection image to create source catalogs in each of the available photometric bands. These catalogs were used to search for Y-band dropouts as described in Section 3.2. In this process signal-to-noise (S/N) was estimated using isophotal apertures (*ISOMAG*) whereas total magnitudes are estimated in scalable Kron apertures (*AUTOMAG*).

This approach follows the well-established procedure adopted and described by Bradley et al. (2012), and we refer to this work for further details.

3.2. Selecting $z \sim 8$ Galaxy Candidates in BoRG13

The selection of the high redshift LBGs closely follows Trenti et al. (2011) and Bradley et al. (2012). We use an identical Y-band dropout selection scheme, i.e., we require that

$$S/N_{V\text{-band}} < 1.5 \quad (1)$$

$$S/N_{J\text{-band}} > 5.0 \quad (2)$$

$$S/N_{H\text{-band}} > 2.5 \quad (3)$$

$$(Y - J) > 1.75 \quad (4)$$

$$(J - H) < 0.02 + 0.15 (Y - J - 1.75), \quad (5)$$

in each of the fields from Table 1. The colors are insensitive to whether isophotal, Kron or aperture magnitudes are used (Finkelstein et al. 2010; Trenti et al. 2012b). Candidates passing these selection criteria have been vetted by visual inspection to remove false positives such as hot pixels and diffraction spike features from bright objects.

As in our previous work, the *SExtractor* stellarity index was used as an additional criterion to help reject stars as potential contaminants. For the J-band 8σ sources the stellarity index is quite reliable and we required it to be < 0.85 . For sources with $5\sigma < S/N_J < 8\sigma$, the stellarity index is more noisy and therefore we did not imply a strict cut, but we used it as a criterion in combination with visual inspection. Three of the authors (KBS, TT, MT) inspected all the dropouts independently with the aim of rejecting spurious or star-like features. After the initial independent classification each dropout was discussed by the three co-authors resulting in the consensus list given in this paper. Only a few objects did not initially get rejected by all authors. These were potential

TABLE 1
BoRG13 SURVEY FIELDS, EXPOSURE TIMES, AND 5σ LIMITING MAGNITUDES^a

Field	α_{J2000} [deg]	δ_{J2000} [deg]	F606W		F098M		F105W		F125W		F160W		Area	E(B−V)
			t [s]	m_{lim}	t [s]	m_{lim}	t [s]	m_{lim}	t [s]	m_{lim}	t [s]	m_{lim}	[$''^2$]	
BoRG_0456-2203	73.9646	-22.0489	2647	26.58	3718	26.75	1809	26.74	1809	26.52	3.06	0.038
BoRG_0951+3304	147.7003	33.0737	2660	26.43	4518	26.43	2212	26.52	2212	26.20	1.82	0.013
BoRG_0952+5304	147.9448	53.0714	2506	26.78	3912	26.69	1806	26.77	1806	26.50	3.72	0.011
BoRG_1059+0519	164.7039	5.3125	2386	26.43	3812	26.72	1806	26.83	1806	26.38	2.15	0.028
BoRG_1118-1858	169.4101	-18.9726	8514	26.94	13235	27.13	6276	27.17	6276	26.94	2.04	0.050
BoRG_1358+4326	209.4754	43.4338	2451	26.77	3812	26.77	1606	26.83	1606	26.47	3.86	0.008
BoRG_1358+4334	209.4636	43.5610	4866	27.02	7023	27.21	3812	27.32	3812	27.06	2.71	0.007
BoRG_1416+1638	214.0048	16.6269	3112	26.86	5271	26.84	2462	26.85	2462	26.55	3.64	0.020
BoRG_1429-0331	217.3717	-3.5185	9164	26.96	13235	27.06	5726	27.00	5726	26.79	3.37	0.083
BoRG_1437+5043_r1	219.2153	50.7244	13570	27.15	19720	26.98	11394	27.04	10691	26.66	1.66	0.013
BoRG_1437+5043_r2 ^b	219.2153	50.7244	13570	27.70	19720	27.65	8885	27.21	11394	27.74	10691	27.49	1.67	0.013
BoRG_1437+5043_r3 ^b	219.2153	50.7244	13570	27.54	19720	27.42	8885	27.14	11394	27.54	10691	27.39	1.52	0.013
BoRG_1459+7146	224.7501	71.7638	3724	26.61	6023	26.75	2812	27.04	2812	26.82	2.78	0.027
BoRG_1510+1115	227.5371	11.2415	13315	27.19	21059	27.43	9529	27.67	9529	27.16	1.78	0.046
BoRG_2132-1202	322.9467	-12.0397	2656	26.20	3718	26.19	1809	26.23	1809	26.00	1.21	0.062
BoRG_2313-2243	348.2326	-22.7252	8308	26.98	13335	27.11	6326	27.11	6326	26.91	3.26	0.026

NOTE. — ^a 5σ magnitude limits are for $r = 0.32''$ apertures corrected for Galactic extinction. The total effective search area for Y-band dropouts in BoRG13 is 40.26 arcmin². The combined effective search area for Y-band dropouts in BoRG09 + BoRG12 + BoRG13 is ~ 247 arcmin². ^bInclude follow-up observations from November 2012 (GO 12905, PI: Trenti) described in Appendix A.

hot pixels being mistaken for real sources in the drizzled un-dithered BoRG data and potential stars (point-like sources). In the former case disagreement led to exclusion from the final sample whereas objects were revisited to obtain agreement in the latter case. We note that the final list therefore includes potential real-source contaminants. However, invoking a relatively high fiducial contamination fraction of the dropout sample as described in Section 4.2 this is accounted for when inferring the intrinsic luminosity function.

The new dataset includes 11 sources passing our selection criteria. 9 of these are new findings, while two (BoRG_1437+5043_r2_637 and BoRG_1510+1115_1218) are candidates initially presented by Trenti et al. (2011) and Bradley et al. (2012) and are now confirmed at higher S/N by the deeper data. The sample of BoRG13 $z \sim 8$ galaxy candidates is summarized in Table 2. In Figures 2 and 3 we show $3'' \times 3''$ postage stamps of all 11 BoRG13 redshift 8 galaxy candidates.

Combining the BoRG13 sample with the updated samples from BoRG09 and BoRG12 results in a total sample of 38 bright $> 5\sigma$ galaxy candidates at $z \sim 8$ from the BoRG survey. Note that a ' 5σ ' detection in this context means $S/N > 5$. As we discuss in Appendix B, the noise background distribution is highly non-Gaussian with significant broader wings. As discussed in the appendix, our requirement of two-band detections and non-detections at bluer bands, is essential to avoid contaminants, especially in the 5σ sample. 10 of the 38 candidates have $S/N_j > 8$.

3.3. Photometric Redshifts

The Bayesian photometric redshift code BPZ (Benítez et al. 2004; Coe et al. 2006) was run on the photometry for each of the LBG candidates shown in Table 2 providing photometric redshift probability distributions, $p(z)$, for each individual object. In Figures 2 and 3 we show the $p(z)$ obtained using a flat prior on the redshift distribution. In all cases prominent probability peaks are seen at the expected Y-band dropout redshift of 7.4–8.8.

4. ESTIMATING THE LUMINOSITY FUNCTION

In this section we present the Bayesian framework applied to infer the luminosity function parameters. We use the empirical Schechter function (Schechter 1976),

$$\Phi(L) = \frac{\phi^*}{L^*} \left(\frac{L}{L^*} \right)^\alpha \exp \left(-\frac{L}{L^*} \right) \quad (6)$$

(see also Appendix C), as our luminosity function model. Hence, the luminosity function parameters to fit are the faint-end slope, α , the 'knee', L^* , characterizing the transition between the power-law part at the faint end and the exponential cut-off at the bright end of the distribution, and the normalization ϕ^* . As described by, e.g., Bradley et al. (2012) and Oesch et al. (2012) α and L^* are degenerate. This implies that both bright objects (the latter, for instance in case of the BoRG sample) and faint objects are needed to obtain precise estimates of both α and L^* . We will illustrate this degeneracy in Section 5 by applying our framework to a sample of faint LBGs only. The normalization ϕ^* represents the co-moving number density of objects described by the luminosity function. The density is directly related to the total number of high-redshift objects, N_z , in the surveyed volume, V , as described below (Equation (9) and Appendix C).

The framework used to fit the Schechter function in the present study improves on the standard formalism typically adopted to estimate luminosity functions in the literature. In particular we improve on three main issues with luminosity function fitting that seems to have become standard practice in the high redshift community

First of all it is often assumed that the likelihood follows a Poisson distribution (e.g., Bradley et al. 2012; Schenker et al. 2013; McLure et al. 2013; Oesch et al. 2012). As described by Kelly et al. (2008), the Poisson distribution is only an approximation of the formally correct binomial distribution. To the extent that the detection probability is small and the total number of objects in the parent sample is large, the binomial distribution reduces to the Poisson distribution. Hence, in

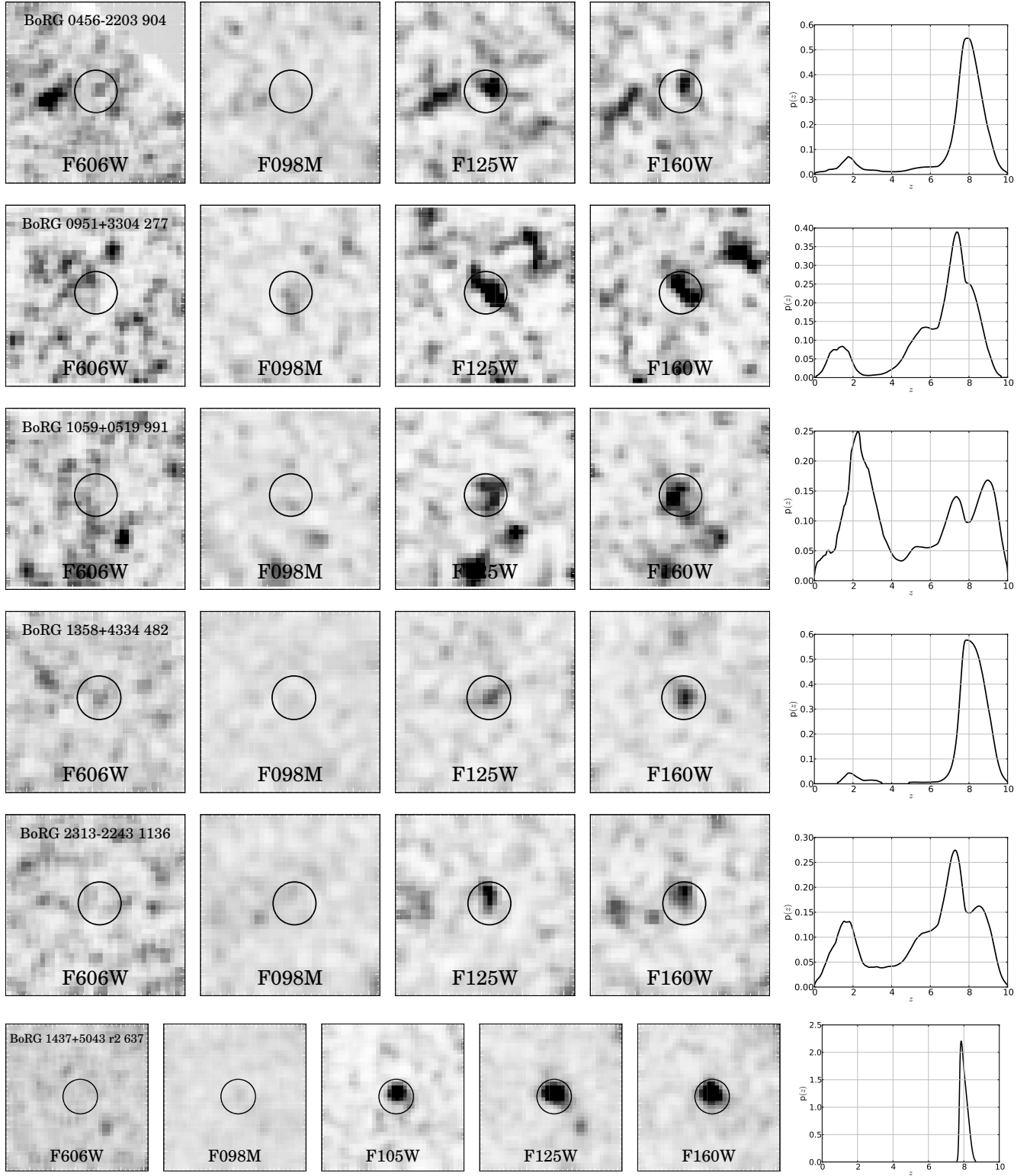


FIG. 2.— 6 of the 11 $z \sim 8$ Y-band dropouts in the BoRG13 sample presented in this paper (the remaining 5 candidates are shown in Figure 3). The first four columns show V-, Y-, J- and H-band $3'' \times 3''$ HST postage stamps with a power-law stretch. The last column shows the photometric redshift probability distribution $p(z)$ (using a flat prior) obtained with the Bayesian redshift code BPZ (Benítez et al. 2004; Coe et al. 2006) for each candidate. In the bottom row the F105W (YJ-band) data from our follow-up campaign of BoRG_1437+5043 (see Appendix A) are included.

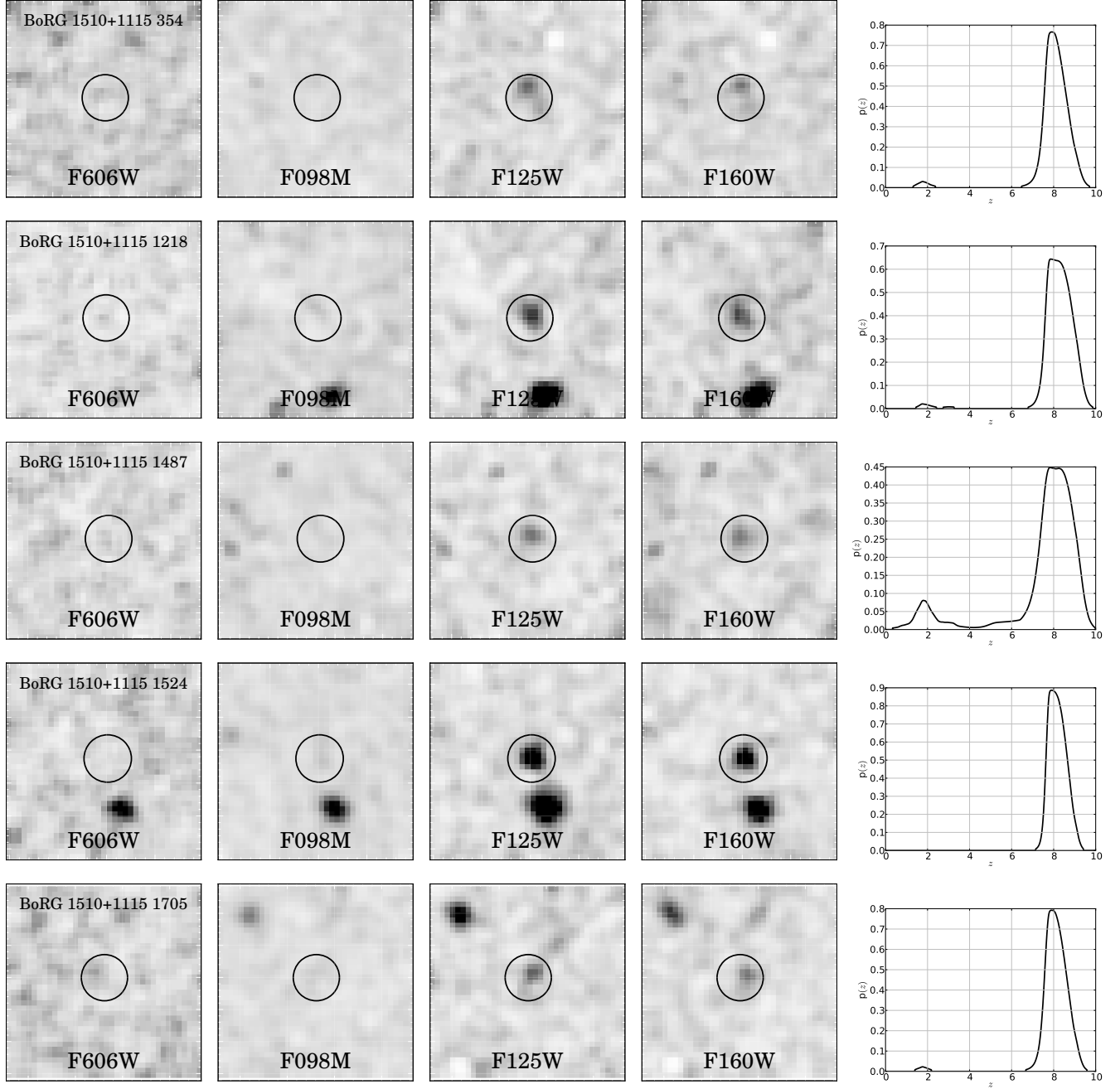


FIG. 3.— The 5 $z \sim 8$ Y-band dropouts in BoRG_1510+1115. The first four columns show V-, Y-, J- and H-band $3'' \times 3''$ HST postage stamps with a power-law stretch. The last column shows the photometric redshift probability distribution $p(z)$ (using a flat prior) obtained with the Bayesian redshift code BPZ (Benítez et al. 2004; Coe et al. 2006) for each candidate.

TABLE 2
PHOTOMETRY OF THE Y-BAND DROPOUT ($z \sim 8$) CANDIDATES IN BoRG13

ID	α_{J2000}	δ_{J2000}	J	Y – J	J – H	S/N _V	S/N _Y	S/N _J	S/N _H
BoRG_0456-2203.904	73.97655	-22.04115	26.72 ± 0.27	2.1 ± 0.9	-0.2 ± 0.4	0.8	0.8	5.1	3.5
BoRG_0951+3304.277 ^a	147.68443	33.07019	25.87 ± 0.22	2.3 ± 0.7	-0.2 ± 0.3	-0.6	1.2	7.9	5.3
BoRG_1059+0519.991	164.69864	5.32262	26.34 ± 0.31	1.8 ± 0.6	-0.2 ± 0.4	0.7	1.6	5.9	3.6
BoRG_1358+4334.482	209.44475	43.55779	26.91 ± 0.26	2.0 ± 0.8	0.0 ± 0.3	1.3	0.4	6.4	4.9
BoRG_1437+5043.r2.637 ^{a,b}	219.21058	50.72601	25.76 ± 0.07	3.2 ± 0.8	0.1 ± 0.1	-0.2	1.0	20.2	16.5
BoRG_1510+1115.354 ^a	227.54706	11.23145	27.03 ± 0.22	2.1 ± 0.7	-0.1 ± 0.3	0.1	1.2	7.7	4.6
BoRG_1510+1115.1218 ^{a,c}	227.54266	11.26152	26.87 ± 0.22	2.2 ± 0.8	0.0 ± 0.3	0.8	0.7	7.3	5.2
BoRG_1510+1115.1487 ^a	227.53173	11.25254	27.60 ± 0.24	2.0 ± 0.8	0.0 ± 0.4	0.4	0.5	5.8	4.0
BoRG_1510+1115.1524 ^a	227.53812	11.25552	26.63 ± 0.15	2.3 ± 0.6	0.0 ± 0.2	-0.8	1.5	11.9	7.9
BoRG_1510+1115.1705 ^a	227.54008	11.25111	27.00 ± 0.19	1.8 ± 0.6	-0.8 ± 0.4	-2.0	1.6	8.4	2.6
BoRG_2313-2243.1136	348.24871	-22.71342	27.14 ± 0.26	2.3 ± 0.8	-0.1 ± 0.3	-0.3	1.0	6.4	4.8

NOTE. – J-band magnitudes are corrected for galactic extinction using the Cardelli et al. (1989) extinction law and the E(B–V) from Table 1. ^aFollowed up with MOSFIRE as presented in Treu et al. (2013). ^bPresented in Trenti et al. (2011) and Bradley et al. (2012) as BoRG58_1787-1420 and BoRG_1437+5043.1137, respectively. For previous photometry of this candidate see the ‘B1437.r2.0637.T12a’ rows in Table 5. ^cPresented in Bradley et al. (2012) as BoRG_1510+1115.1404. The HST postage stamps and the photometric redshift probability distribution $p(z)$ for each candidate are shown in Figures 2 and 3.

the case of rare-object luminosity functions the Poisson distribution is a fair approximation. Effects like cosmic variance (Schenker et al. 2013) will further smear and reduce any significant differences and we therefore do not expect any strong bias in the shape of the luminosity function from this approximation. Nevertheless it is important to quantify this statement, by applying the formally correct binomial distribution, and verify that this is indeed not the case.

Secondly, it has become generally accepted to use binned samples of dropouts when estimating the luminosity functions (e.g., Bouwens et al. 2006, 2007, 2011; Bradley et al. 2012; McLure et al. 2013; Schenker et al. 2013) instead of using the actual data themselves. Such an approach intentionally reduces the information to an arbitrarily defined set of bins which is sub-optimal and introduces smoothing on the scale of the bins thus potentially biasing the inference to flatter distributions (Cara & Lister 2008; Yuan & Wang 2013).

Lastly, the photometric errors on the individual sources in the high-redshift samples are often not modeled directly when obtaining the luminosity function parameters. Bouwens et al. (2007, 2011) use a set of generalized transfer functions to model the effect of photometric scatter in their samples and simulations similar to the ones described in Section 4.1 are used to account for photometric scatter in and out of the color selection boxes (Bradley et al. 2012; Oesch et al. 2012), or between adjacent bins in the binned luminosity function (Schenker et al. 2013). However, due to the binning of the data when fitting the luminosity function this does not fully account for the photometric uncertainty of the individual objects in the sample. Certainly previous approaches provided an approximate treatment, but direct modeling of the photometric uncertainties themselves makes full use of all the available information and provides more rigorous results.

The formalism applied in this study is therefore drawing from a posterior distribution using a likelihood based on the binomial distribution described by Kelly et al. (2008), avoiding binning of the data completely and thereby estimating the luminosity function using the full information directly, and lastly, explicitly modeling the

photometric error distribution of the sample by assuming the errors are Gaussian distributed.

The posterior distribution for n Y-band dropouts can be summarized as (see Appendix C)

$$\begin{aligned}
 p(\theta \mid L_{J,\text{obs}}, I_V = 0) &\propto p(\theta) \\
 &\times C_{(1-f)n}^{N_z} C_{fn}^{\frac{f}{1-f}N_z} \prod_l^C \left[1 - \frac{A_l}{A_{\text{sky}}} p(I = 1|\theta) \right]^{\frac{N_z - (1-f_l)c_l}{1-f_l}} \\
 &\times \prod_i^n p(L_{J,\text{obs},i}|\theta)
 \end{aligned} \tag{7}$$

Here $\theta = (\alpha, L^*, N_z)$ where α and L^* are the main Schechter luminosity function parameters and N_z is the number of high- z LBGs in the surveyed co-moving cosmological volume, which as mentioned is closely related to ϕ^* , the Schechter function normalization. $L_{J,\text{obs}}$ is the set of observed J-band luminosities and $I_V = 0$ indicates that the object is a V-band non-detection as required by the dropout selection described in Section 3.2. On the right-hand-side $p(\theta)$ represents the prior assumptions on the problem and the C_b^a factors are binomial coefficients. We assume uniform priors on α , $\log_{10} L^*$ and $\log_{10} N_z$. $p(I = 1|\theta)$ is the probability distribution of an object making it into the dropout sample which is independent of the n individual objects in the sample, and $p(L_{J,\text{obs},i}|\theta)$ is the likelihood function for the observed J-band luminosity of the i 'th object in the sample. A_l is the area of the individual C fields in the BoRG13 sample, which each contain c_l high redshift candidates ($n = \sum_l^C c_l$) and have an assumed contamination of f_l . A_{sky} is the area of the full sky. In Appendix C we give the expanded expression of the posterior distribution from Equation (7) which was actually used when performing the luminosity function parameter inference. We note that in the current framework the $p(z)$ prior on the redshift of the individual LBG candidates is not explicitly taken into account. We refer to Appendix C for further details.

A posterior distribution function as the one shown in Equation (7) is well suited for Markov Chain Monte Carlo (MCMC) sampling over the luminosity function parameters θ . Calculating the posterior probability en-

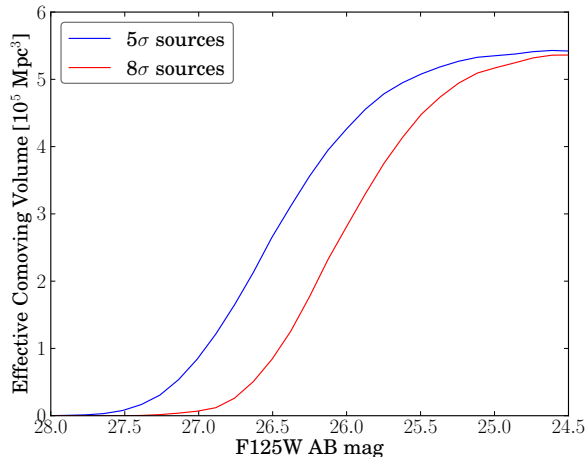


FIG. 4.— The effective co-moving volume of BoRG13 as a function of J-band (F125W) magnitude for the 5σ (blue) and 8σ (red) sample. This is calculated taking the selection functions $S(L_{J,\text{obs}}, z)$ and completeness functions $C(L_{J,\text{obs}})$ described in Section 4.1 of each individual field into account.

ables a robust determination of the luminosity function as preferred by the data given the sample of n sources. We used the Python `pymc` package² with a Robust Adaptive Metropolis (RAM; Vihola 2012) algorithm to sample the luminosity function parameters α , L^* , and N . The RAM algorithm adapts the proposal covariance matrix to obtain a fixed acceptance ratio (set to 0.4 in this work).

4.1. Selection and Completeness Functions

When estimating the luminosity function a crucial part of the expression for the posterior distribution is the selection function $\mathcal{S}(L_{J,\text{obs}})$ including an estimate of the completeness of the source selection. Here we have used two distinct selection functions.

For each of the BoRG fields we explicitly split the total selection function into a completeness function $C(L_{J,\text{obs}})$ and a selection function not including completeness $S(L_{J,\text{obs}}, z)$. $C(L_{J,\text{obs}})$ and $S(L_{J,\text{obs}}, z)$ were simulated as described by Oesch et al. (2007, 2009, 2012) and Bradley et al. (2012). In summary, the steps in obtaining these functions are:

- Sources with different spectral energy distribution, luminosity, redshift, and size are added to the original science images. The simulated galaxies are $z \sim 4$ galaxies rescaled to higher redshift using a size relation of $(1+z)^{-1}$ as determined from $z \sim 3 - 7$ LBG samples (Bouwens et al. 2004; Ferguson et al. 2004; Oesch et al. 2010a) and their UV-continuum slopes (Dunlop et al. 2012a; Finkelstein et al. 2012; Bouwens et al. 2012).
- The detection and selection procedure described in Section 3 is re-run for each field to determine $C(L_{J,\text{obs}})$ and $S(L_{J,\text{obs}}, z)$.

The selection function $\mathcal{S}(L_{J,\text{obs}})$ (used in Section C.2) is as mentioned corrected for completeness. When estimating the intrinsic luminosity function the BoRG13

LBGs are all assumed to be at $z = 8$. Hence, when sampling the posterior for the BoRG fields

$$\mathcal{S}(L_{J,\text{obs}}) = C(L_{J,\text{obs}}) \times S(L_{J,\text{obs}}, z = 8). \quad (8)$$

The effective volume of the BoRG survey is derived from the full selection function as a function of J-band magnitude, i.e., $C(L_{J,\text{obs}}) \times S(L_{J,\text{obs}}, z)$. The total effective co-moving volumes for the 5σ and 8σ BoRG13 samples are shown in Figure 4

To break the α - L^* parameter degeneracy we used a sample of 59 faint LBGs from the Hubble Ultra Deep Field (HUDF) and Early Release Science (ERS) programs (Tables 14–17 in Bouwens et al. 2011) to populate the faint end of the distribution when fitting the luminosity function. For this sample a piecewise selection function $\mathcal{S}(L_{J,\text{obs}})$ following the binned data presented in Bouwens et al. (2011) was used. Integration over this selection function was done using linear interpolation between the bins. Note that the effect of large-scale structures (cosmic variance) on the $z = 8$ luminosity functions in the HUDF/ERS luminosity range is very modest as described by Bouwens et al. (2011).

Both the BoRG and HUDF/ERS selection function models $\mathcal{S}(L_{J,\text{obs}})$ are explicitly set to 1 and 0 for luminosities brighter than and fainter than the modeled luminosities, respectively.

4.2. Contamination

When estimating the number of contaminants among the BoRG LBG candidates we follow the approach taken by Bradley et al. (2012). We use a fiducial average contamination level of $f_{\text{BoRG}} = 0.42$ for the BoRG sample. (In Section 5.1 we investigate the effects of modifying this assumption on the shape of the luminosity function) The contamination of the HUDF/ERS sample is included in the selection function described above and is therefore assumed to be 0.0 for the Bouwens et al. (2011) sample. The available information about the contaminants at redshift 8 is limited and distinguishing between the luminosity function of the contaminants and the $z \sim 8$ LBGs complicates matters considerably. Hence, we assume that the fraction of contaminants is independent of luminosity for the BoRG sample. In Equation (7) The number of contaminants are approximated by their expectation values as explained in Appendix C.

Having obtained N_z and assuming that the luminosity function does not evolve over the redshift interval of interest, the number density is obtained by calculating (see Equation (C4) in Appendix C)

$$\phi^* = \frac{N_z}{V \times \int_{L_{\min}}^{\infty} \frac{1}{L^*} \left(\frac{L}{L^*}\right)^{k-1} \exp\left(-\frac{L}{L^*}\right) dL}. \quad (9)$$

Here V is the co-moving cosmological volume of the ideal full-sky survey. To avoid divergence of the integral we set our lower integration limit of the luminosity function to $L_{\min} = 10^{40}$ erg/s which corresponds to an absolute magnitude of $M \sim -10$. Hence, L_{\min} sets the lower bound for what we include as “a galaxy” in our analysis. With an estimated normalization of the sample luminosity function, the luminosity density, ϵ , is obtained by integrating the luminosity function multiplied by the luminosity itself (see Appendix C).

² Available at <http://pymc-devs.github.io/pymc/>

4.3. Sanity Check of Bayesian Framework

Prior to applying the newly developed Bayesian inference framework to the BoRG13 data it was tested extensively on a set of simulated data samples. We confirmed that in all cases the MCMC sampling recovered the input luminosity functions from which the emulated samples were drawn. We also tested the code on the $z \sim 8$ LBG sample analyzed in Bradley et al. (2012) (BoRG12). The obtained luminosity function had a faint-end slope of $\alpha = -2.06^{+0.27}_{-0.25}$ and $M^* = -20.40^{+0.36}_{-0.45}$ in agreement with the $\alpha = -1.98^{+0.23}_{-0.22}$ and $M^* = -20.26^{+0.29}_{-0.34}$ presented by Bradley et al. (2012). Within the 1σ confidence intervals these measurements of both α and M^* are fully consistent. We note that we do not expect the results to be identical, since our framework avoids some of the approximations of previous studies.

5. RESULTS

From the framework described in Section 4 the assumed intrinsic luminosity function for a sample of objects can be determined. In the following we will describe and summarize our findings from applying our framework to the 97 $z \sim 8$ LBG candidates from the combined samples of BoRG13 and HUDF/ERS from Bouwens et al. (2011). We note that to ease comparison with the literature we convert L^* into M^* in the remainder of this work using that $M^* = M_{UV\odot} - 2.5 \log_{10}(L^*/L_{\odot})$ with $M_{UV\odot} = 5.48$.

5.1. The Luminosity Function at $z \sim 8$ from BoRG13

We apply the inference framework to the full BoRG13 sample of 38 objects augmented by the fainter 59 candidates presented in Bouwens et al. (2011). For a consistency check on a more robust determination of the luminosity function bright end, we also consider a restricted BoRG13 sample consisting of the 10 objects in BoRG13 detected at $S/N_{J\text{-band}} > 8$, similarly to the approach followed by Bradley et al. (2012). This additional step allows us to validate the luminosity function derived from the full sample, which might be affected by photometric scatter as discussed in Appendices A and B.

When sampling the posterior distribution (given in Appendix C Equation (C15)) we use the selection functions described in Section 4.1, i.e., interpolation over a piecewise selection function for the HUDF/ERS data from Bouwens et al. (2011) and the simulated selection and completeness functions for the 5σ and 8σ BoRG samples at $z = 8$.

The results from sampling θ after an MCMC burn-in phase are shown in Figure 5. From top to bottom we show the results from fitting the Schechter luminosity function to the BoRG13 5σ , BoRG13 8σ (both including the Bouwens et al. (2011) sample), and the Bouwens et al. (2011) samples. The latter is presented to illustrate the prominent degeneracy between the α and M^* luminosity function parameters without the bright BoRG LBGs to constrain the bright end of the distribution and break the degeneracy. The 1σ and 2σ confidence intervals are indicated by the red contours.

In Table 3 the results from the full BoRG13 luminosity function and the BoRG13 luminosity function only using the 8σ candidates are summarized together with a selection of recent luminosity function fits from the lit-

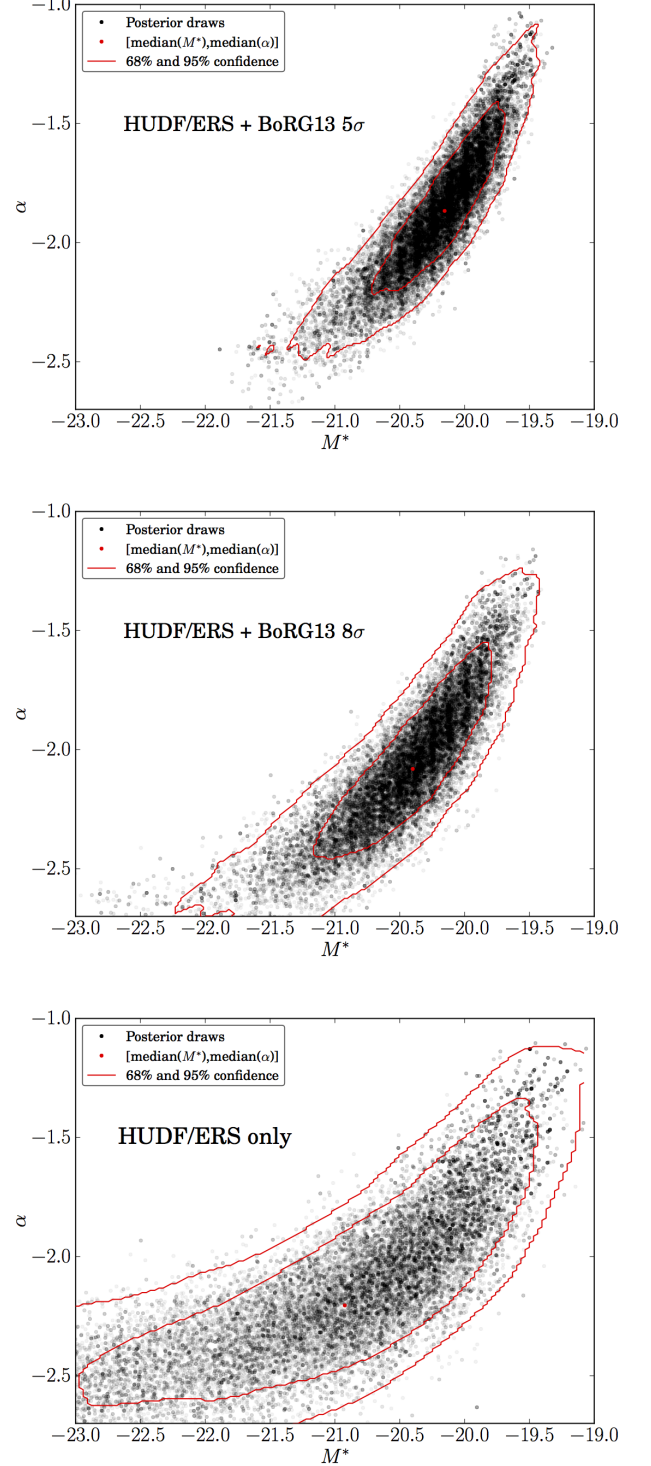


FIG. 5.— The MCMC draws (black dots) from inferring the luminosity function parameters α and M^* based on candidate $z \sim 8$ LBG samples. Here L^* has been converted to absolute magnitude M^* to ease comparison with the literature. From top to bottom results from the BoRG13 5σ sample, the BoRG13 8σ sample, both including the Bouwens et al. (2011) faint HUDF/ERS $z \sim 8$ LBG sample, and the Bouwens et al. (2011) sample only is shown. The latter clearly illustrates the degeneracy between α and M^* . Adding the bright BoRG Y-band dropouts greatly improve the α and M^* estimates. The best-fit BoRG13 values (small red dots) agree well with the sample of literature luminosity functions presented in Table 3. Contours show 68.2% and 95.4% (1σ and 2σ) confidence intervals.

TABLE 3
COMPARISON OF LUMINOSITY FUNCTION PARAMETERS

Reference	M^*	α	$\log_{10} \phi^* [\text{Mpc}^{-3}]$	$\log_{10} \epsilon [\text{erg/s/Hz/Mpc}^3]$
BoRG13 5 σ sample (This work)	$-20.15^{+0.29}_{-0.38}$	$-1.87^{+0.26}_{-0.26}$	$-3.24^{+0.25}_{-0.34}$	$25.52^{\text{a}}_{-0.05}$
BoRG13 8 σ sample (This work)	$-20.40^{+0.39}_{-0.55}$	$-2.08^{+0.30}_{-0.29}$	$-3.51^{+0.36}_{-0.52}$	$25.50^{\text{a}}_{-0.06}$
Bradley et al. (2012)	$-20.26^{+0.29}_{-0.34}$	$-1.98^{+0.23}_{-0.22}$	$-3.37^{+0.26}_{-0.29}$	25.50^{a}
Oesch et al. (2012)	$-19.80^{+0.46}_{-0.57}$	$-2.06^{+0.45}_{-0.37}$	$-3.17^{+0.40}_{-0.55}$	$25.58^{\text{b}} \pm 0.12$
Bouwens et al. (2011)	-20.10 ± 0.52	-1.91 ± 0.32	$-3.23^{+0.74}_{-0.27}$	$25.65^{\text{b}} \pm 0.11$
Lorenzoni et al. (2011)	-19.5	-1.7 (fixed)	-3.0	25.23^{c}
Trenti et al. (2011)	-20.2 ± 0.3	-2.0 (fixed)	-3.4 (fixed)	25.45^{a}
McLure et al. (2010)	-20.04 (fixed)	-1.71 (fixed)	-3.46	25.17^{a}
Bouwens et al. (2010)	-19.5 ± 0.3	-1.74 (fixed)	-2.96 (fixed)	$25.18^{\text{d}} \pm 0.24$
Schenker et al. (2013)	$-20.44^{+0.47}_{-0.33}$	$-1.94^{+0.21}_{-0.24}$	$-3.50^{+0.35}_{-0.32}$	25.46^{a}
McLure et al. (2013)	$-20.12^{+0.37}_{-0.48}$	$-2.02^{+0.22}_{-0.23}$	$-3.35^{+0.28}_{-0.47}$	25.46^{a} (but see their Figure 7)

NOTE. – ^aEstimated from the luminosity function parameters via the method described in Appendix C integrated down to $M = -17.7$ at $\lambda = 1600\text{\AA}$ using $M_{\text{UV}\odot} = 5.48$. A small $\sim 0.13\text{dex}$ offset between these estimates and the literature was found. This difference can be recovered using $M_{\text{UV}\odot} \sim 4.7$ suggesting that a value similar to this was used in, e.g., Oesch et al. (2012); Bouwens et al. (2011) and McLure et al. (2013). ^bFrom Oesch et al. (2012) and Bouwens et al. (2011), respectively, where the luminosity function was integrated down to $M = -17.7$ for $\lambda = 1600\text{\AA}$. ^cFrom Lorenzoni et al. (2011) where the luminosity function was integrated down to $M = -18.5$ for $\lambda = 1600\text{\AA}$. ^dFrom Bouwens et al. (2010) where the luminosity function was integrated down to $M = -18.2$ for $\lambda = 1700\text{\AA}$.

erature. The BoRG13 luminosity function parameters α and M^* agree well with the literature values, confirming that the Poisson approximation is indeed a fair approximation when fitting luminosity functions at $z \sim 8$, in terms of best-fit value. We note that the BoRG13 5 σ best-fit faint-end slope is fully consistent within the $1\text{-}\sigma$ error bars with the literature values. We also note that the BoRG13 5 σ faint-end slope of -1.87 is fully consistent with the faint-end slope obtained from the BoRG12 data using the framework presented here ($\alpha = -2.06$) within the 1σ error bars and fall comfortably within the 68% confidence interval contour when also considering the degeneracy with M^* in the top panel of Figure 5.

The luminosity functions corresponding to each of the MCMC samples shown in Figure 5 are compared to the literature luminosity functions from Table 3 in Figure 6.

The relatively shallow best-fit faint-end slope of -1.87 for the BoRG13 5 σ sample might question the speculated steepening of the luminosity function at $z > 6$. Such a steepening is expected from galaxy formation models and cosmological simulations (Trenti et al. 2010; Jaacks et al. 2013; Tacchella et al. 2013), and would be related to the evolution of the slope of the dark matter halo mass function at the scale of $M_h \sim 10^{10} M_\odot$ which is characteristic for hosting the faint galaxies observed in the HUDF. To place our latest determination of $\alpha(z = 8)$ in the broader context of other studies, Figure 7 shows the redshift evolution predicted by a recent theoretical models (e.g., Tacchella et al. 2013; Cai et al. 2014), together with estimated UV luminosity function faint-end slopes at $z \sim 0.7 - 2.5$ (Oesch et al. 2010a), $z \sim 2 - 3$ (Reddy & Steidel 2009), $z \sim 4$ (Bouwens et al. 2007), $z \sim 4 - 7$ (Bouwens et al. 2012), and $z \sim 7$ (Bouwens et al. 2011). As the error bars on our $z \sim 8$ α -estimate are still fairly large with $\Delta\alpha = 0.26$ a potential decline is still very possible within 1σ . Even though cosmic variance is insignificant over the full BoRG13 sample, it is important to check that it does not have a significant effect on the estimate of the faint-end slope, which is based on only three quasi-independent fields (HUDF). Based on the calculations by Trenti & Stiavelli (2008), the additional uncertainty due to cosmic variance is $\Delta\alpha \sim 0.08$,

which is small compared to the statistical uncertainty of our study, and therefore can be neglected.

This all highlights that significantly larger samples of faint as well as bright redshift 8 galaxies are needed to robustly determine the luminosity function shape and to confirm the suggested steepening of $\alpha(z)$ with redshift. We note that the more robust BoRG13 8 σ sample has a steeper faint-end slope and therefore favors a steepening of α despite the marginally larger error bars compared to the BoRG13 5 σ sample.

From the MCMC samples of θ we estimate the number density of high redshift objects, ϕ^* , and the luminosity density, ϵ , using the expressions given in Section 4.2 and Appendix C. The distributions of the obtained ϕ^* and ϵ values for the BoRG13 5 σ and 8 σ samples are shown in Figure 8. The median estimates and their uncertainties are quoted in Table 3. The ϵ values were obtained by integrating down to the HUDF magnitude limit of $M = -17.7$ (Bouwens et al. 2011). Integrating to fainter magnitudes, i.e., extrapolating outside the data range, increases the luminosity density itself as well as the uncertainties.

In Figure 9 we present the full multi-dimensional parameter space α , M^* , ϕ^* , and ϵ for the BoRG13 5 σ MCMC inference (the lower left plot reproduces the top panel in Figure 5 and the ϕ^* and ϵ probability distribution functions are also shown in the top row of Figure 8). This illustrates the strong correlations between the three luminosity function parameters. As can be seen there is no significant correlation between the luminosity density, ϵ , and the luminosity function parameters when integrating down to $M = -17.7$, i.e., it is well-determined. Extrapolating ϵ (or rather the luminosity function) to fainter magnitudes introduces strong correlations.

As noted in Section 4.2 we have used a fiducial contamination fraction of 42% for the BoRG sample following Bradley et al. (2012). In the presented Bayesian framework the assumed contamination affects both the shape and the normalization of the luminosity function. To quantify this effect we estimated the luminosity function for the BoRG13 5 σ sample using a contamination fraction of $f_{\text{BoRG}} = 0.0, 0.2, 0.33, 0.5, 0.55$, and 0.6 (the same

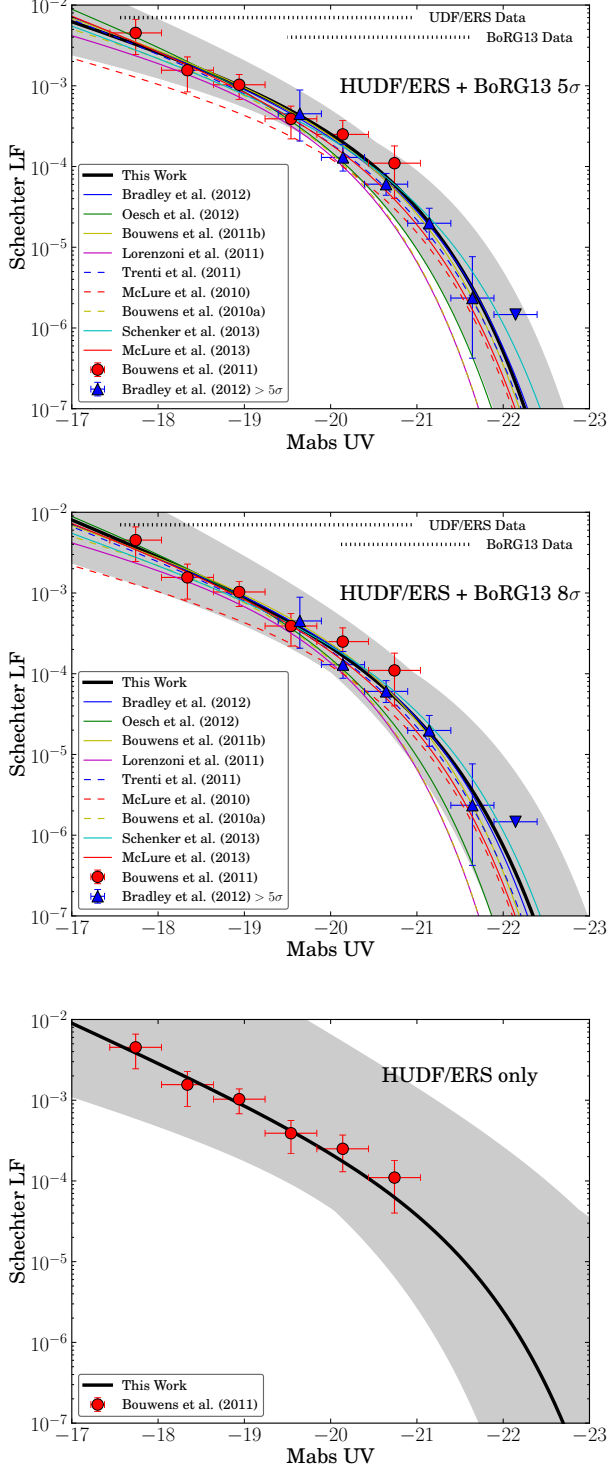


FIG. 6.— The BoRG13 luminosity function (black solid line) corresponding to the median values of the MCMC samples shown in Figure 5 for the BoRG13 5σ sample and the BoRG13 8σ sample both including the Bouwens et al. (2011) faint HUDF/ERS $z \sim 8$ LBG sample are shown in the two top panels. The dotted lines indicate the ranges the BoRG13 5σ sample and the HUDF/ERS Bouwens et al. (2011) sample span. Each luminosity function is compared to a sample of luminosity functions from the literature (see Table 3). The binned data from BoRG12 (Bradley et al. 2012) and HUDF/ERS (Bouwens et al. 2011) are shown for reference as the blue and red symbols, respectively. We emphasize that we are *not* fitting to these binned data. We take advantage of the full information of the data sets by using the full unbinned BoRG13 data. In the bottom panel the resulting luminosity function using only the faint HUDF/ERS Bouwens et al. (2011) sample is shown. The gray shaded regions in all three panels show the 68% confidence intervals of the MCMC draws. The BoRG13 Schechter luminosity functions are seen to agree well with the literature luminosity functions.

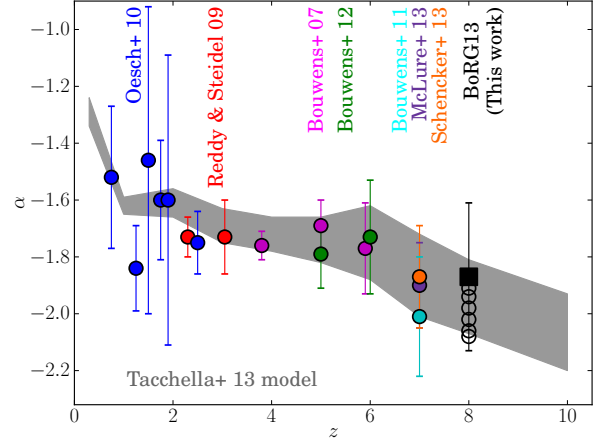


FIG. 7.— The luminosity function faint-end slope α as a function of redshift. The references of the individual points are indicated above the points. The shaded region shows the physical model of the faint-end-slope evolution from Tacchella et al. (2013). The square at $z \sim 8$ shows the result presented here for the 5σ sample. The open circles at redshift 8 show the literature faint-end slopes (without error-bars not to clutter the plot) from Table 3 for comparison. The uncertainties are too large to confirm or reject the suggested steepening of the luminosity function at $z \gtrsim 7$.

values used in Table 8 of Bradley et al. 2012). The resulting luminosity functions parameters are summarized in Table 4. The BoRG13 5σ luminosity function parameters are presented in Table 3. The effect on the characteristic magnitude and the number density of high-redshift objects is smaller than the estimated 1σ uncertainty with only 0.09 dex and 0.15 dex difference between the two extrema. The faint-end slope varies by 0.27 from no contamination to a contamination of 60% which is comparable to the average 1σ uncertainty on the slope. The variations in the luminosity function parameters found here are similar to the range in parameters found by Bradley et al. (2012). Hence, our more detailed calculations confirm that validity of previous approaches.

To summarize, in general the luminosity function parameters estimated using the BoRG13 sample are in good agreement with previous results within the 1σ uncertainties (see Table 3).

5.2. Inferences About Reionization

Having derived rigorous posterior distribution functions for the parameters describing the luminosity function at $z \sim 8$ we are in a position to infer the implications of our measurement for reionization. Before proceeding with this inference we briefly summarize the basic equations describing the problem. We refer to Shull et al. (2012) and Robertson et al. (2013) and references therein for more details. The fraction of ionized hydrogen Q depends on the balance between the density of ionizing photons n_{ion} and the recombination time t_{rec} as

$$\dot{Q} = \frac{n_{\text{ion}}}{\langle n_{\text{H}} \rangle} - \frac{Q}{t_{\text{rec}}} . \quad (10)$$

The density of ionizing photons can be related to the measured UV luminosity density ϵ given a conversion factor ξ based on models for the spectral energy distribution of the sources and the ionizing photons escape fraction

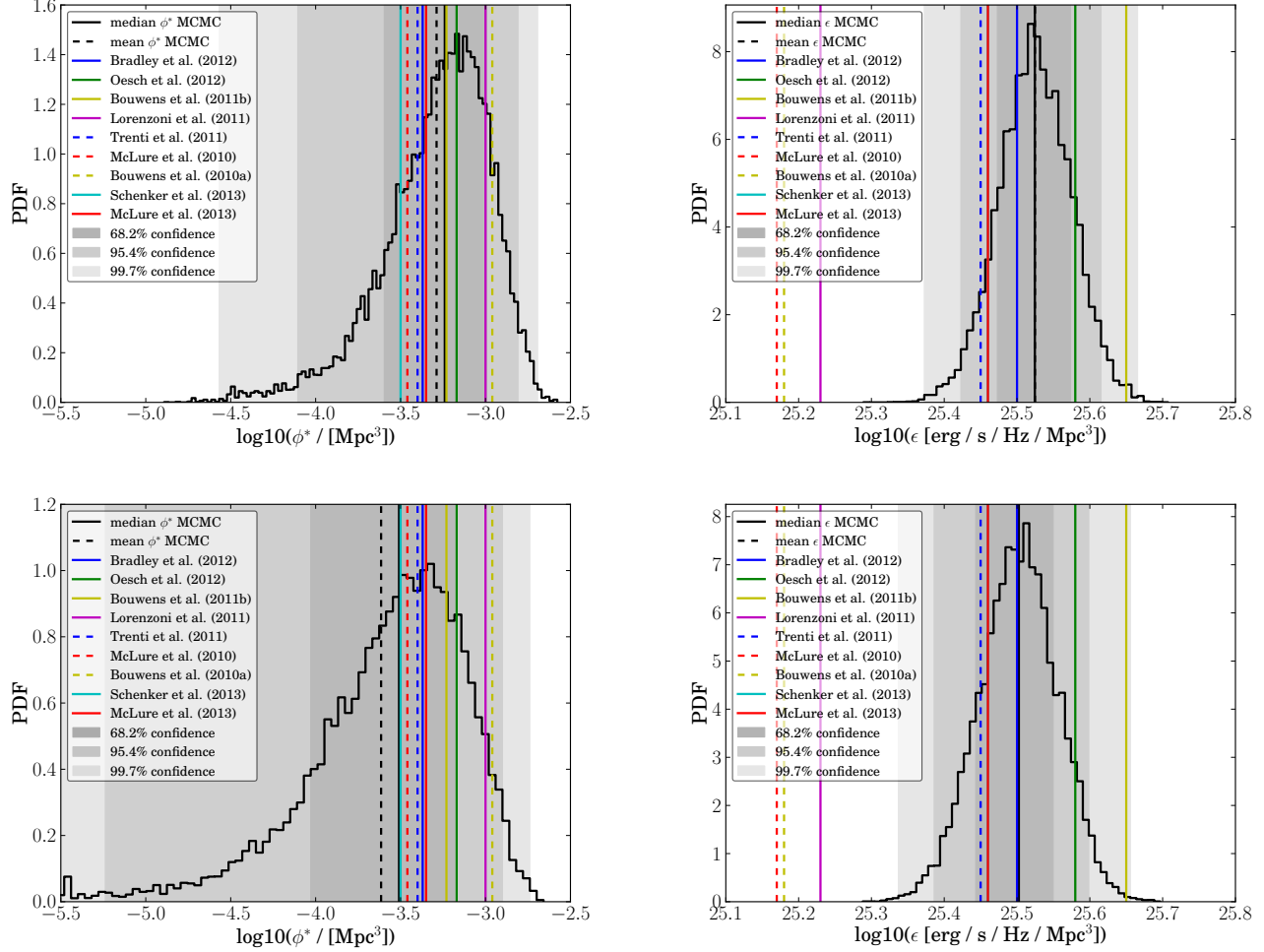


FIG. 8.— The probability distribution functions (PDF) of the number density ϕ^* (left column) and luminosity density ϵ (right column) of $z \sim 8$ LBGs estimated as described in Section 4.2 (and Appendix C) from the BoRG13 5σ (top) and BoRG13 8σ (bottom) samples. The shaded regions show the confidence intervals of the distributions. The mean and median values are indicated by the dashed and solid black vertical lines. ϕ^* and ϵ values from the literature (Table 3) are shown by the remaining vertical lines according to the legends. Again the agreement between the results obtained here and in the literature is prominent.

TABLE 4
EFFECT OF CONTAMINATION FRACTION ON LUMINOSITY FUNCTION ESTIMATE

f_{BoRG}	M^*	α	$\log_{10} \phi^* [\text{Mpc}^{-3}]$	$\log_{10} \epsilon [\text{erg/s/Hz/Mpc}^3]$
0.00	$-20.23^{+0.30}_{-0.39}$	$-1.73^{+0.27}_{-0.26}$	$-3.17^{+0.23}_{-0.32}$	$25.57^{+0.05}_{-0.05}$
0.20	$-20.18^{+0.30}_{-0.37}$	$-1.76^{+0.26}_{-0.26}$	$-3.19^{+0.24}_{-0.32}$	$25.55^{+0.05}_{-0.05}$
0.33	$-20.17^{+0.29}_{-0.35}$	$-1.82^{+0.26}_{-0.25}$	$-3.22^{+0.24}_{-0.31}$	$25.54^{+0.05}_{-0.05}$
0.42 [†]	$-20.15^{+0.29}_{-0.38}$	$-1.87^{+0.26}_{-0.26}$	$-3.24^{+0.25}_{-0.34}$	$25.52^{+0.05}_{-0.05}$
0.50	$-20.15^{+0.29}_{-0.35}$	$-1.92^{+0.27}_{-0.25}$	$-3.27^{+0.26}_{-0.32}$	$25.51^{+0.05}_{-0.05}$
0.55	$-20.15^{+0.29}_{-0.38}$	$-1.96^{+0.26}_{-0.25}$	$-3.30^{+0.26}_{-0.35}$	$25.51^{+0.05}_{-0.05}$
0.60	$-20.14^{+0.29}_{-0.38}$	$-2.00^{+0.27}_{-0.25}$	$-3.32^{+0.27}_{-0.36}$	$25.49^{+0.05}_{-0.05}$

NOTE. — [†]Fiducial contamination used in this study as presented in Table 3.

f_{esc} :

$$n_{\text{ion}} = \xi \epsilon f_{\text{esc}}. \quad (11)$$

At $z = 8$, for case-B³ recombination of hydrogen at 20,000K and taking the baryon physical density from WMAP9 (Planck differs by only $\sim 1\%$), the condition

³ Case-B recombination is for an opaque IGM as opposed to case-A recombinations which relates to an IGM transparent to Ly α radiation as described by Baker & Menzel (1938).

for ionization equilibrium $\dot{Q} = 0$ can be expressed as:

$$\log_{10} \left(\frac{QC}{f_{\text{esc}}} \right) = \log_{10} \epsilon + \log_{10} \xi - 50.31 \quad (12)$$

where C is the so-called clumping factor ($\langle n_{\text{H}}^2 \rangle / \langle n_{\text{H}} \rangle^2$), ϵ is the luminosity density in units of $\text{erg s}^{-1} \text{Hz}^{-1} \text{Mpc}^{-3}$, and ξ is given in Hz/erg . Typically, some fiducial value is assumed for the unknowns in order to determine whether the observed galaxies are sufficient to keep the Universe

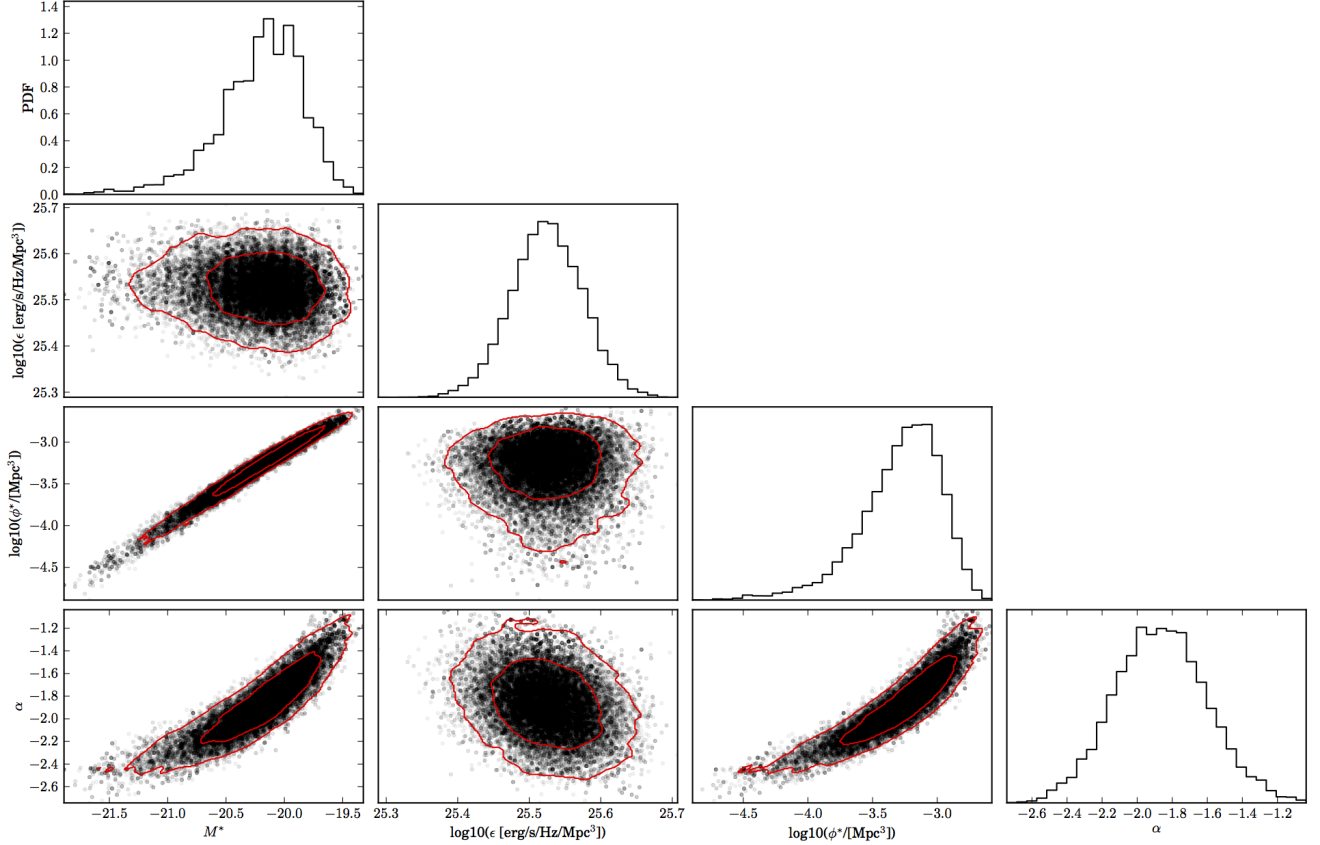


FIG. 9.— The correlations between the faint-end slope, α , the characteristic magnitude, M^* , the number density of redshift 8 LBGs, ϕ^* , and the luminosity density, ϵ , integrated down to the HUDF limit of $M = -17.7$ (Bouwens et al. 2011) estimated from the BoRG13 5σ sample. The marginalized one-dimensional probability distribution function (PDFs) of each parameter is shown in the upper right panels. The red contours show the 1σ and 2σ confidence contours. Prominent correlations are seen between the three luminosity function parameters α , M^* , and ϕ^* , whereas no correlation is seen with ϵ as it is integrated down to $M = -17.7$, i.e., over the actual range of the data. Integrating down to fainter magnitudes will introduce a correlation and increase the mean luminosity density value as well as the uncertainties on the estimate. The lower left panel reproduces the top panel in Figure 5 and the PDFs of ϕ^* and ϵ are shown in the top row of Figure 8.

ionized and, in case they are not, to explore if extrapolation of the observed luminosity function to fainter magnitudes is sufficient to increase the ionized fraction of hydrogen to that level.

We carry out our inference by assigning prior probabilities to the unknowns based on theoretical considerations. ξ depends on metallicity, the initial mass function age and the dust content of the stellar populations. Based on the measured UV slopes by Dunlop et al. (2012b) and a range of models, Robertson et al. (2013) estimate it to be in the range $\log_{10} \xi [\text{Hz/erg}] = 24.75\text{--}25.35$ and take 25.2 as their fiducial value. We describe the range of theoretically accepted values as a lognormal distribution with mean 25.2 and standard deviation 0.15 dex.

Figure 10 shows the inferred value of QC/f_{esc} for the BoRG13 5σ luminosity function as a function of the integration limit when estimating ϵ , M_{lim} . As the average luminosity density grows as the integration limit is pushed to ever fainter magnitudes the overall value of QC/f_{esc} increases. The horizontal lines indicate the ionized fraction of hydrogen for fixed C and f_{esc} . We use $C = 3$ (e.g., McQuinn et al. 2011; Shull et al. 2012; Finlator et al. 2012; Kaurov & Gnedin 2013) and $f_{\text{esc}} = 0.2$ (e.g., Ouchi et al. 2009; Shull et al. 2012; Robertson et al. 2013) as our fiducial values. The vertical line shows the

HUDF limit from Bouwens et al. (2011) corresponding to the distribution of ϵ shown in the top right panel of Figure 8. It is clear from Figure 10 that only when integrating all the way down to $M = -12$ Q is well below 1 for fixed C and f_{esc} . Hence, for $C = 3$ and $f_{\text{esc}} = 0.2$ it seems unlikely that the $z \sim 8$ population of Y-band dropouts are capable of keeping the Universe fully ionized.

We can make further progress by adopting a prior on C/f_{esc} . Recent theoretical calculations suggest that C is of order 1-6, and we therefore assume a uniform prior within this range. Very little empirical or theoretical information is available on the escape fraction. We formalize the uncertainty on this parameter by assuming a uniform prior in the range $f_{\text{esc}} \in [0.1 - 0.5]$ (e.g., Fernandez & Shull 2011). With these priors we derive the joint constraints on Q and M_{lim} shown in Figure 11. Figure 11 shows that allowing for a larger range in C and f_{esc} increases the available ranges of Q for the BoRG13 luminosity function. However, even here only for the most extreme combination of C and f_{esc} at $M \sim -15$ there seems to be enough radiation available to sustain a fully ionized Universe at $z \sim 8$. Overall it is clear from Figures 10 and 11 that reionization is far from being completed at $z \sim 8$ by an LBG population following the

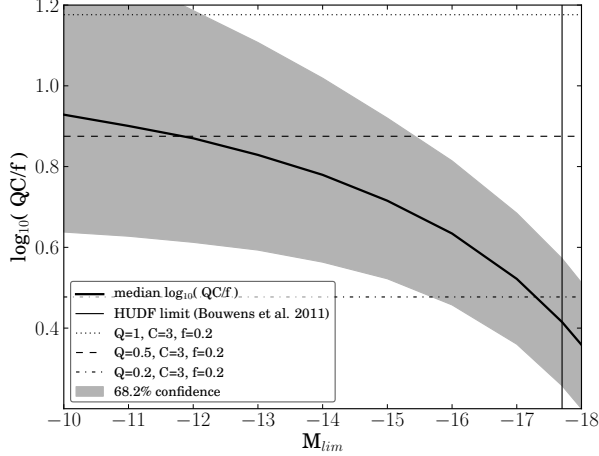


FIG. 10.— The inferred value of QC/f_{esc} as a function of the limiting magnitude M_{lim} which the BoRG13 5σ luminosity density is integrated down to. The horizontal lines show the fraction of ionized hydrogen for fixed clumping factor, C , and photon escape fraction, f_{esc} , according to the legend. The vertical line shows the HUDF limit of -17.7 from Bouwens et al. (2011).

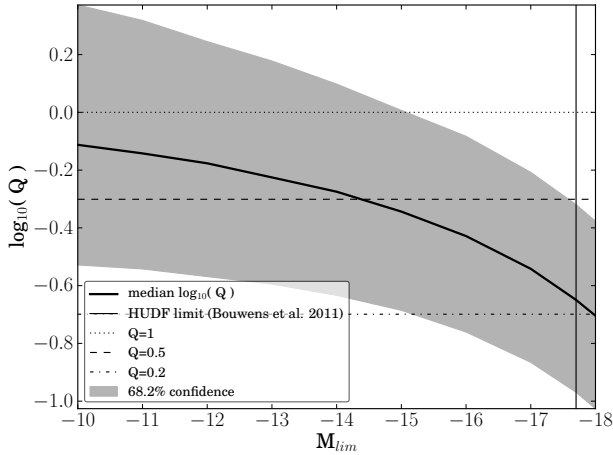


FIG. 11.— The inferred value of Q as a function of the limiting magnitude M_{lim} assuming a flat prior on the clumping factor $C \in [1 - 6]$ and the photon escape fraction $f_{\text{esc}} \in [0.1 - 0.5]$. The horizontal lines show an ionization fraction of 20%, 50% and 100%. The vertical line shows the HUDF limit of -17.7 from Bouwens et al. (2011). The prior on C and f_{esc} allows for a fully ionized Universe, but only if objects all the way down to $M \sim -15$ are included. There is very little change to keep the Universe fully ionized if only galaxies down to the HUDF limit are considered.

BoRG13 5σ luminosity function. Invoking a luminosity function with a steeper faint-end slope (e.g., the BoRG13 8σ luminosity function) changes this picture somewhat. However, $Q \sim 1$ still requires radiation from objects down to $M \sim -16$, as supported by non-detection of gamma-ray burst host galaxies at $z > 5$ (Trenti et al. 2012a; Tanvir et al. 2012) and therefore still supports a late reionization, i.e., that reionization completes at $z < 8$.

We can compare our inference on Q with the values inferred from the measured Ly α optical depth as inferred from spectroscopic follow-up of Y-band dropouts (e.g., Treu et al. 2013). Naturally this comparison is extremely

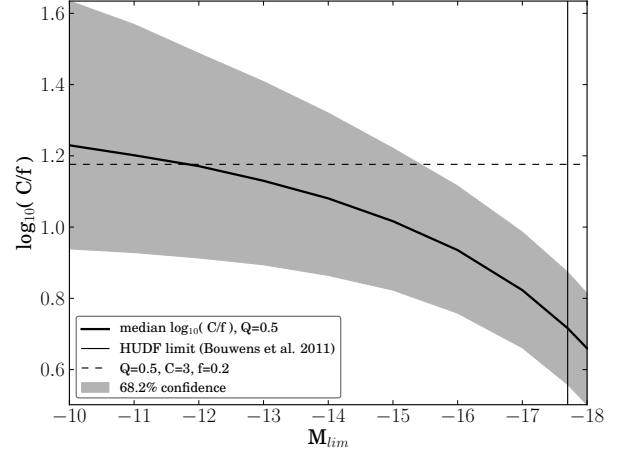


FIG. 12.— The inferred value of C/f_{esc} as a function of the limiting magnitude M_{lim} assuming $Q = 0.5$ for the BoRG13 5σ luminosity function. The horizontal dashed line shows where $C = 3$ and $f_{\text{esc}} = 0.2$. As in Figures 10 and 11 the vertical line marks the HUDF limit.

delicate and needs to rely on a number of assumptions, as the Ly α optical depth depends not only on the average fraction of neutral hydrogen in the IGM but also on the details of the Ly α emission itself and on the detailed radiative transfer at or in the vicinity of the source (e.g., Dijkstra et al. 2011; Bolton & Haehnelt 2013). Several authors have suggested that ionized fractions of ~ 0.5 are needed to explain the observed decline in Ly α emission from LBGs between $z \sim 6$ and $z \sim 7$, if all the optical depth arises from neutral hydrogen in the IGM and if the universe is completely reionized by $z \sim 6$. Our recent follow-up of a subsample of the BoRG LBGs with MOSFIRE (Treu et al. 2013) indicates that the optical depth increases even more out to $z \sim 8$, indicating perhaps an even lower fraction of ionized hydrogen, which seems to be in good agreement with the results summarized in Figures 10 and 11. However, given the extreme assumptions, these numbers should be considered lower limits to the cosmic average fraction of neutral hydrogen. In order to gain some insight into C/f_{esc} we can adopt $Q = 0.5$ as our upper limit and infer our exclusion plots in C/f_{esc} versus M_{lim} shown in Figure 12.

In summary the inferred luminosity function from the BoRG13 5σ data is not capable of fully ionizing the Universe at redshift $z \sim 8$ as a significant fraction of neutral hydrogen seems to still be present. This is in good agreement with recent results from spectroscopic follow-up campaigns which all seem to suggest that a significant fraction of neutral hydrogen is present at $z > 7$. Hence, the results presented here support a late reionization scheme where the reionization is still ongoing at $z \sim 8$.

6. SUMMARY AND CONCLUSION

The BoRG survey has carried out the largest-area search to date for Y-band dropouts (HST F098M-dropouts). We present new observations from 12 parallel fields not included in our previous studies and additional deeper datasets for two fields. We combine our BoRG sample with a sample of fainter dropouts taken from the literature and use the combined sample of 97 dropouts

to carry out a rigorous study of the luminosity function at $z \sim 8$ and its implications for reionization. Our main results can be summarized as follows:

1. We present 9 new Y-band dropouts from the ~ 50 arcmin² of new data. Furthermore, we re-confirm two dropouts previously presented by Trenti et al. (2011) and Bradley et al. (2012). Combining these 11 dropouts with out previously published $z \sim 8$ LBGs from BoRG gives a sample of 38 bright ($25.5 \leq m_J \leq 27.6$) redshift 8 LBGs from the BoRG survey.
2. We develop and implement an improved method for estimating the luminosity function parameters for a sample of n galaxies. Using a Bayesian framework the posterior distribution of the population based on a binomial distribution is given. Combining the BoRG Y-band dropouts with the faint $z \sim 8$ LBGs from HUDF/ERS presented by Bouwens et al. (2011) and sampling over this posterior distribution enables a robust recovery of the faint-end slope, α , the characteristic magnitude of the Schechter function, M^* , the normalizing number density of $z \sim 8$ LBGs, ϕ^* , and the luminosity density, ϵ , of the redshift 8 luminosity function.
3. The inferred luminosity function at $z \sim 8$ is described by the parameters:

$$\begin{aligned} M^* &= -20.15^{+0.29}_{-0.38}, \\ \alpha &= -1.87^{+0.26}_{-0.26}, \\ \log_{10} \phi^* [\text{Mpc}^{-3}] &= -3.24^{+0.25}_{-0.34}, \\ \log_{10} \epsilon \left[\frac{\text{erg}}{\text{s Hz Mpc}^{-3}} \right] &= 25.52^{+0.05}_{-0.05} \end{aligned}$$

Here ϵ is the inferred UV luminosity density integrated down to the HUDF limit $M_{\text{lim}} = -17.7$.

Our inferred credible intervals include recent estimates of the same parameters.

4. We show that for the BoRG13 $z \sim 8$ luminosity function the average fraction of ionized hydrogen Q is only of the order 10-50% for samples down to the HUDF limit of $M = -17.7$ assuming standard values of the clumping factor and the photon escape fraction. To sustain a fully ionized Universe at redshift 8 with the presented luminosity function it is necessary to account for the radiation of objects as faint as $M = -15$.
5. The inferred ionization fractions suggest a relatively late reionization scenario where a considerable fraction of neutral hydrogen is still present at $z \sim 8$ in good agreement with the results of our recent spectroscopic MOSFIRE campaign (and others from the literature) where we followed up a subsample of the BoRG redshift 8 LBGs presented here.

The inference on the implications of the BoRG13 luminosity function for reionization presented here are still limited by the sizable error bars at redshift 8. To reduce the uncertainties on the inferred quantities bright and faint galaxy samples from e.g., the Frontier Fields and future parallel HST campaigns are crucial.

This work was supported by the HST BoRG grants GO-11700, 12572, and 12905. This paper is based on observations made with the NASA/ESA Hubble Space Telescope, obtained at the Space Telescope Science Institute. BK acknowledges support from the Southern California Center for Galaxy Evolution, a multi-campus research program funded by the University of California Office of Research. Support for this work was provided by the European Commission through the Marie Curie Career Integration Fellowship PCIG12-GA-2012-333749 (MT).

APPENDIX

A. HST-GO FOLLOW-UP OF BORG_1437+5043

The BoRG_1437+5043 field is a special case, and thus its analysis deserves a detailed description. The field was originally identified by Trenti et al. (2012b) as an overdensity of 4 Y-band dropouts detected above the 5σ limit and 1 detected above 8σ . As explained in that work, overdensities of high redshift galaxies are expected to occur from theoretical and numerical dark matter modeling. It was thus argued that the overdensity could potentially be a high redshift protocluster. Bradley et al. (2012) subsequently carried out a re-analysis of the field. With improved data reduction and photometry algorithms, 2 out of the 4 initial 5σ candidates presented by Trenti et al. (2012b) fell below the formal 5σ threshold. The 8σ candidate was confirmed.

In order to further investigate the nature of the sources in this field, follow-up observations were proposed for and obtained in November 2012. The main goal of the new HST campaign (GO 12905, PI: Trenti) was to look for fainter members of the overdensity as well as expand the area surveyed by centering the field directly on the overdensity. The GO data was taken in the 4 original photometric bands of the BoRG survey, F606W, F098M, F125W, and F160W, plus F105W in order to sharpen the redshift estimate of the dropout candidates. In Figure 13 we show the combined J-band image of BoRG_1437+5043. The three differently colored regions mark regions with similar depth and band coverage. The filters used in each region are listed. Regions 1 and 2 outline the original area of the BoRG_1437+5043 field analyzed by Trenti et al. (2012b). Regions 2 and 3 show the position of the new data. Hence, region 2 centered on the potential protocluster contains the deepest data.

The new GO observations were reduced and analyzed together with the rest of the BoRG13 data as presented in this paper. Each of the three regions were analyzed independently in order to accommodate the different depth and band coverage. The limiting magnitudes of each of the three regions are listed in Table 1 together with the rest of the BoRG13 fields. Photometry at the location of the five sources identified by Trenti et al. (2012b) is given in Table 5.

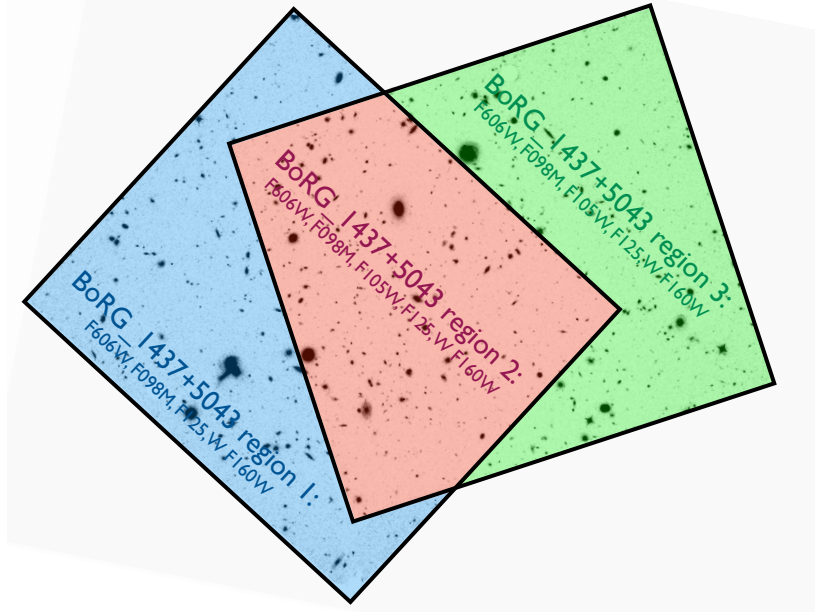


FIG. 13.— The combined J-band imaging of the original and follow-up observations of BoRG_1437+5043. The coloring shows the 3 regions used when analyzing the photometry of the drizzled image and mark regions with comparable depth and band coverage. Region 1 and 2 outline the observations presented and analyzed in Trenti et al. (2012b) and Bradley et al. (2012). The data obtained in November 2012 is outlined by region 2 and 3 which was centered on the potential protocluster presented in Trenti et al. (2012b).

We note that the two dropouts that were not confirmed in the reanalysis carried out by Bradley et al. (2012) are indeed not high- z candidates according to the deeper data, thus confirming the improvements introduced in the BoRG pipeline.

Postage stamps at the location of the three candidates retained by Bradley et al. (2012) are shown in Figure 14 along with their photometric redshift estimates. As we can see from the photo- z estimates, 2 of the 3 candidates are confirmed to be at $z \sim 8$, even though one of them (T12e) falls just outside of the formal Y-H color selection criterion. T12a is now detected at $S/N > 20(16)$ in the J(H) band and T12e is detected at $S/N > 9(7)$. They are thus both excellent $z \sim 8$ redshift candidates. The third candidate (T12b) is undetected in the deeper data and thus we conclude it was a spurious noise peak. The beautifully sharp photo- z of the initial 8σ candidate T12a is a nice validation of the reliability of the high-significance sample where $S/N_J > 8$. As we show in the next section the distribution of noise and background is highly non-Gaussian, so it is not surprising that a fraction of sources just above the 5σ threshold are spurious. The 2/3 confirmed fraction is consistent with the fiducial contamination fraction of 42% that we adopt in our inference based on numerical simulations.

Albeit, with admittedly small number statistics this follow-up campaign validates our approach of carrying out separately the inference for the more robust 8σ detections and comparing the results with those based on the 5σ sample for which contamination is expected to be higher. No fainter candidates are detected in the field. These results imply that the field is still likely to be an overdensity of $z \sim 8$ but not as pronounced as previously thought.

B. NON-GAUSSIAN NOISE DISTRIBUTION AND THE IMPORTANCE OF MULTI-BAND SELECTION

When quoting ‘ 3σ ’ or ‘ 5σ ’ detections in dropout surveys, as well as other areas of astrophysics, it may be implicitly assumed that the noise of the science images is Gaussian distributed such that a 3σ and 5σ detection corresponds to a probability of the detection being real of 99.730020% and 99.999943%. For a million independent apertures, like those in the BoRG survey, this would correspond to 2700 and 0.57 objects, respectively, and thus effectively no contaminants in a 5σ sample, even for an area as large as the one surveyed by BoRG.

In practice, however, we do not expect the noise distribution to be Gaussian. Furthermore, we do not expect it to be symmetric. This is in part due to unresolved background objects but also due to the positive nature of defects such as faint cosmic ray hits and hot pixels. Thus, when the data are pushed to the limit as in dropout searches for Lyman break galaxies, the non-Gaussian tails of the noise distributions can result in false positive detections (e.g., Dunlop 2013) even if they are formally 5σ detections.

In this appendix we take advantage of the very large area covered by the BoRG Survey to characterize and demonstrate the non-Gaussianity of the background. We show that the level of contaminants is much higher than for a Gaussian background, and that only through the use of multiple filters for detections and non-detection requirements it can be kept at the relatively manageable level of 42%.

We construct the actual probability distribution function of background noise by conducting aperture photometry on all 10^6 possible apertures of radius $r = 0''.32$ from the empty regions in 71 of the BoRG fields. Empty regions are identified according to the SExtractor segmentation maps (grown by 5 pixels) produced when creating our source catalogs as described in Section 3. We note that the correlated noise introduced by the drizzling of the science images

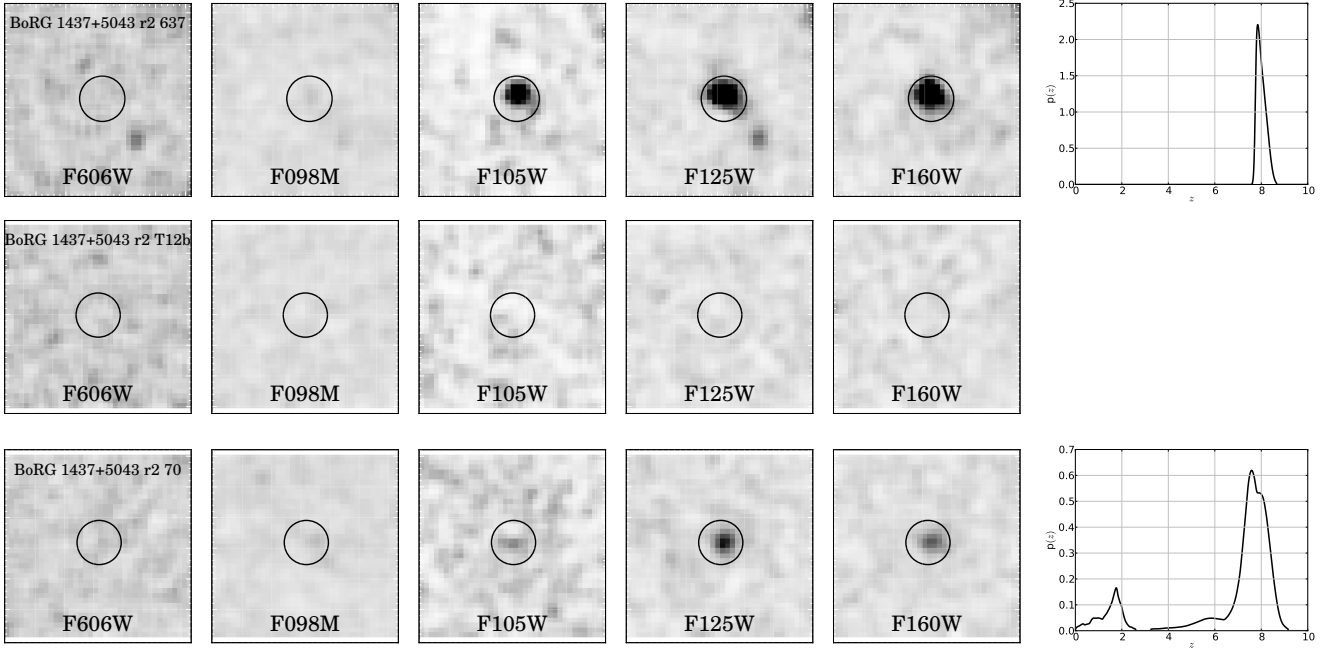


FIG. 14.— Follow-up GO observations of the three high-redshift galaxy candidates in BoRG_1437+5043 (Trenti et al. 2012b, top to bottom shows candidate a, b and e). The first five columns show F606W, F098M, F105W, F125W and F160W $3'' \times 3''$ postage stamps with a power-law stretch. The last column shows the redshift probability distribution $p(z)$ (using a flat prior) obtained with the Bayesian redshift code BPZ (Benítez et al. 2004; Coe et al. 2006) for the two candidates detected in the BoRG13 data. The first row duplicates the bottom row of Figure 2 and is displayed here for completeness.

TABLE 5
BoRG13 PHOTOMETRY OF Y-BAND DROPOUTS IN BoRG_1437+5043 FROM TRENTI ET AL. (2012b)

ID	α_{J2000}	δ_{J2000}	J	Y – J	J – H	S/N _V	S/N _Y	S/N _J	S/N _H	Sample
B1437_r2.0637_T12a	219.21058	50.72601	25.76 ± 0.07	3.19 ± 0.78	0.07 ± 0.11	–0.2	1.0	20.2	16.5	BoRG13
	219.210672	50.7260085	26.1 ± 0.1	> 2.7	0.0 ± 0.2	–1.5	–1.0	10.9	7.9	BoRG12
	219.2107	+50.7260	25.8 ± 0.1	> 2.90	–0.10	–	–	13.0	8.0	BoRG09
B1437_r2.T12b	219.22405*	50.72597*	–	–	–	–	–	–	–	BoRG13
	219.2240496	50.7259683	27.3 ± 0.3	> 1.8	-0.3 ± 0.5	0.3	0.5	5.0	2.7	BoRG12
	219.2241	+50.7260	27.2 ± 0.3	> 1.90	–0.30	–	–	5.1	2.6	BoRG09
B1437_r2.0560_T12c	219.23092	50.72405	27.75 ± 0.23	0.83 ± 0.47	0.06 ± 0.33	3.5	2.6	6.1	5.0	BoRG13
	219.2310489	50.7240585	27.1 ± 0.2	> 1.8	-0.7 ± 0.6	1.1	–0.5	5.0	1.7	BoRG12
	219.2311	+50.7241	26.9 ± 0.2	> 2.00	–0.30	–	–	5.5	2.7	BoRG09
B1437_r2.T12d	219.22027*	50.71563*	–	–	–	–	–	–	–	BoRG13
	219.2202746	50.7156344	27.4 ± 0.3	> 1.8	0.0 ± 0.4	0.6	0.6	4.9	3.3	BoRG12
	219.2203	+50.7156	27.2 ± 0.2	> 1.80	–0.30	–	–	5.4	2.7	BoRG09
B1437_r2.0070_T12e	219.22225	50.70808	26.91 ± 0.14	1.53 ± 0.49	-0.03 ± 0.24	0.8	2.1	9.4	7.0	BoRG13
	219.2223469	50.7080907	27.1 ± 0.2	2.0 ± 0.8	-0.4 ± 0.5	1.0	1.0	5.8	2.8	BoRG12
	219.2224	+50.7081	27.0 ± 0.2	> 2.10	–0.40	–	–	6.0	2.9	BoRG09

NOTE. – Columns are the same as in Table 2 except for the last column which shows where the data were taken from. The ‘T12x’ subscript in the IDs refers to the candidate’s designation in Trenti et al. (2012b) Figure 3. *Coordinates taken from Bradley et al. (2012) as objects are not in the BoRG13 SExtractor segmentation maps.

is automatically accounted for by this approach. In Figure 15 we show the distribution of S/N values for all apertures in the J-band (left) and the J-H-band 2D S/N histogram for objects with $S/N_V < 1.5$ (right). The dashed line in the left panel shows a Gaussian fit to the J-band distribution of the empty apertures. It is clear that the one-dimensional distribution of the noise apertures has broader tails than would be expected for a Gaussian distribution.

The majority of the potential false positives are rejected by our multi-band requirements: a ‘ 5σ ’ detection in J as well as a ‘ 2.5σ ’ detection in the H-band and a non-detection in the V band ($S/N_V < 1.5\sigma$). This selection is illustrated by the box in the upper right corner of the right panel in Figure 15. In spite of the three band selection, still 479 empty apertures survive the cuts, i.e. ~ 7 per BoRG field. The 8σ requirement on J is more stringent but still leaves 65 apertures, i.e. approximately one per BoRG field.

However, as mentioned in Section 3 a crucial part of the dropout selection is the color cut on $Y - J > 1.75$. Applying this stringent cut removes *all* of the noise peaks passing the S/N cuts. This can be understood as the results of two effects in the BoRG data. First, the vast majority of sources in the sky are not as red, and therefore the population

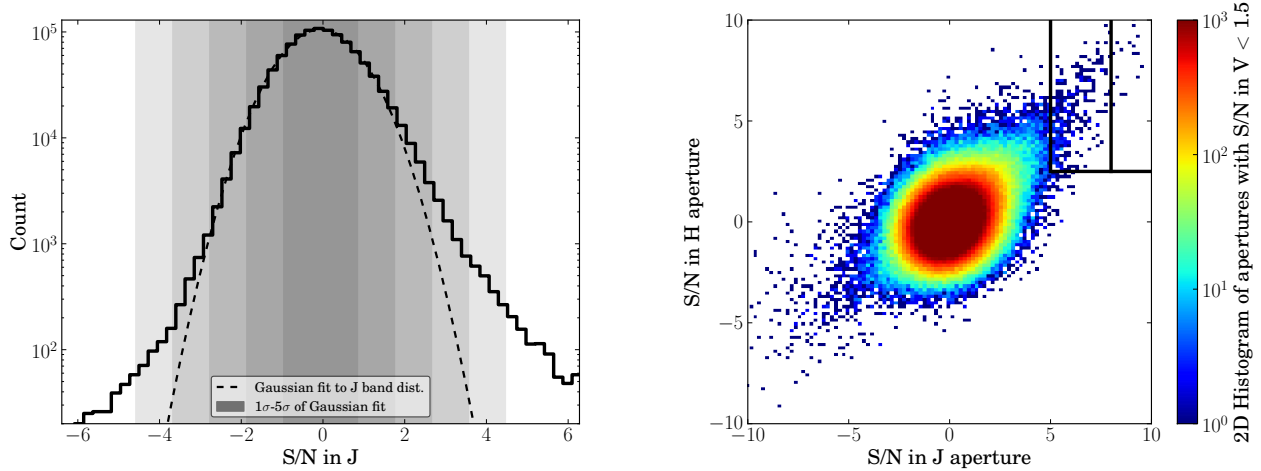


FIG. 15.— The left panel shows the distribution of the measured J-band S/N in 10^6 apertures of “empty sky” from the BoRG fields. The dashed line shows a Gaussian fit to the distribution. It is clear that the wings of the distribution are highly non-Gaussian. In the right panel the 2D distribution in J and H for apertures with $S/N_V < 1.5$ is shown. Again the wings are non-Gaussian giving rise to a relatively high occurrence of spurious high- σ detections. The two boxes in the upper right corner show the region of potentially false positive 5σ and 8σ candidates. Of the 10^6 apertures 479 and 65 fall in these two regions, respectively. Applying the Y–J color cut of the dropout selection described in Section 3 removes all these potential false positives which illustrates the importance of stringent color criteria in dropout searches digging into the noise, like the one presented in this paper.

with fluxes just below our detection threshold which happens to be upscattered in the sample by noise fluctuations is unlikely to satisfy this requirement. Second, spurious positive signals like hot pixels will be present in all near-infrared bands in undithered data and therefore requiring much fainter flux in Y than J helps eliminate those as well. We note that the BoRG survey by design takes all three near-infrared exposures in the same orbit to maximize the chances that hot pixels and detector persistence create images in both the Y-band (taken first), J-band and H-band image. Hence, such artifacts should not be selected as Y-band dropouts in the BoRG survey.

From this study of the noise distribution we draw the following conclusions. Potential contaminants abound in 5σ samples, and multiple band detections are essential to keep them under control. Thus, it is to be expected that repeated observations of the same field will yield different sets of marginal candidates, like in the case of the BoRG_1437+5043 field. Higher significance 8σ samples are much more reliable, but still not immune to noise fluctuation. In addition to carrying out and comparing analyses for both 5σ and 8σ samples it is therefore essential to impose strict color cuts, or impose equivalently tight photo- z requirements. This naturally reduces the completeness of the samples, but it is a reasonable price to pay as long as the completeness can be properly accounted for by means of detailed simulations.

C. BAYESIAN LUMINOSITY FUNCTION INFERENCE FRAMEWORK

In this appendix we outline the Bayesian framework used to infer the parameters of the intrinsic luminosity function in this study. Before describing the posterior distribution used for the MCMC sampling we describe how the individual parameters are related under the assumption of a Schechter luminosity function.

C.1. The Schechter Luminosity Function and its Parameters

The luminosity function of a sample of galaxies represents the density of objects in a given co-moving volume as a function of the luminosity. Hence, it gives information about the population of galaxies at a certain redshift and can be integrated to reveal the total number of galaxies. For luminosity functions at higher redshift this becomes interesting as this gives a direct measure of the reionization power of the galaxies at the given epoch and therefore aid the understanding of which sources reionized the Universe and by how much and when the majority of reionization happened. The Schechter function (Schechter 1976) is one of the most widely used luminosity function models. The Schechter function is given by

$$\Phi(L) = \frac{\phi^*}{L^*} \left(\frac{L}{L^*} \right)^{k-1} \exp \left(-\frac{L}{L^*} \right) \quad (C1)$$

where k is the so-called shape parameter. $k - 1 = \alpha$ is the so-called ‘faint-end slope’ of the luminosity function that is analyzed in the present study. L^* is the scale parameter that determines the transition between the power-law behavior of Equation (C1) that dominates at low luminosities and the exponential cut-off at the bright end. ϕ^* is a normalizing co-moving number density of objects. The Schechter function is closely related to the gamma distribution as

$$\text{gamma}(L|k, L^*) = \frac{\Phi(L)}{\phi^* \Gamma(k)} = \frac{\left(\frac{L}{L^*} \right)^{k-1} \exp \left(-\frac{L}{L^*} \right)}{L^* \Gamma(k)} \quad (C2)$$

with $\Gamma(k)$ being the gamma function which is defined as

$$\Gamma(k) = \int_0^\infty \left(\frac{L}{L^*}\right)^{k-1} \exp\left(-\frac{L}{L^*}\right) d\frac{L}{L^*}. \quad (\text{C3})$$

Formally the integral of the gamma (Schechter) function diverges for $k < 0$. This problem is circumvented by introducing a minimum luminosity, L_{\min} , instead of integrating from 0. As the concept of galaxies is only valid above a certain luminosity this approximation is physically motivated. For instance a galaxy of $L_{\text{gal}} = L_\odot$ makes no physical sense. An often used “definition” of a galaxy is an object with an absolute magnitude $M_{\text{abs}} > -10$ which corresponds to a luminosity of $L \sim 10^{40} \text{ erg/s}$ which is roughly 10^6 times the energy output of the Sun. Limiting the integration of the gamma functions makes it the *incomplete* gamma function.

The normalizing galaxy density, ϕ^* , is closely related to the total number of galaxies present in the surveyed volume of the Universe following the given luminosity function. As noted above, the luminosity function can be integrated to reveal the total number of galaxies, N , within the effective co-moving volume V given the number density ϕ^* such that

$$\begin{aligned} N &= V \times \int_{L_{\min}}^\infty \Phi(L) dL \\ &= V \times \int_{L_{\min}}^\infty \frac{\phi^*}{L^*} \left(\frac{L}{L^*}\right)^{k-1} \exp\left(-\frac{L}{L^*}\right) dL \end{aligned} \quad (\text{C4})$$

which assumes that the luminosity function does not evolve over the considered redshift interval. The effective co-moving volume can be determined as

$$V = \int \frac{dV}{dz} p(z) dz \quad (\text{C5})$$

where $\frac{dV}{dz}$ is the cosmological volume element and $p(z)$ is the probability of selecting the objects for a given redshift in the surveyed redshift range; essentially a selection function. For an evolving luminosity function the integral in Equation (C4) is done over $\frac{dV}{dz}$ separately.

In a similar manner it is possible to obtain the luminosity density, ϵ , i.e., the available radiation per volume, radiated by the galaxy sample, by integrating the product of the luminosity function and the luminosity such that

$$\epsilon = \int_{L_{\min}}^\infty \Phi(L) \times L dL \quad (\text{C6})$$

Hence, the three key parameters to determine when characterizing the luminosity function of a sample of galaxies are k , L^* and N (or similarly α , M^* and ϕ^*). In the following we will described the marginal posterior distribution we used to obtain these parameters.

C.2. The Marginal Posterior Distribution

From Bayesian statistics it is known that the posterior probability distribution is proportional to the product of the prior distribution and the likelihood. When determining the luminosity function of samples of high redshift objects, what is usually done is essentially to assume that everything is detected above a certain luminosity threshold, which in the case of the $z \sim 8$ objects we deal with here, is the detection threshold in the J-band, under the assumption that each object is not detected in V. Thus the relationship between the posterior and prior probability distribution for the high-redshift galaxy candidates can be expressed as

$$p(\theta \mid L_{\text{J,obs}}, I_V = 0) \propto p(\theta) \times p(L_{\text{J,obs}}, I_V \mid \theta) \quad (\text{C7})$$

where the last term is the likelihood. $\theta = (k, L^*, N_z)$ contains the parameters describing the luminosity function $\Phi(L)$, $L_{\text{J,obs}}$ is the observed luminosity in the J-band with $L_{\text{J,true}}$ being the true luminosity, and I_V indicates whether the observed luminosity in the V-band $L_{\text{V,obs}}$ represents a formal detection ($I_V = 1$) or not ($I_V = 0$). For an object to be included in the sample it cannot be detected in the V-band so $p(I_V = 0 \mid L_{\text{J,obs}}, \theta) = 1$ is always the case. $p(\theta)$ contains any prior information on the luminosity function parameters that might be available. In the present study we assume uniform priors on α , $\log_{10} L^*$ and $\log_{10} N_z$.

Expanding the expression for the posterior in Equation (C7) marginalizing over the nuisance parameter $L_{\text{J,true}}$ (the true luminosity of the object in the J-band) leads to a *marginal* posterior probability distribution for a sample of n galaxies which is given by (see Section 3.1 and Appendix B of Kelly et al. 2008):

$$\begin{aligned} p(\theta \mid L_{\text{J,obs}}, I_V = 0) &\propto p(\theta) C_{n_z}^{N_z} \prod_l^C [1 - A_l/A_{\text{sky}} p(I = 1 \mid \theta)]^{N_z - c_{lz}} \times \prod_i^{n_z} p(L_{\text{J,obs},i} \mid \theta) \\ &C_{n_c}^{N_c} \prod_l^C [1 - A_l/A_{\text{sky}} p(I = 1 \mid \theta)]^{N_c - c_{lc}} \times \prod_i^{n_c} p(L_{\text{J,obs},i} \mid \theta) \end{aligned} \quad (\text{C8})$$

where N_z is the number of high- z sources in the Universe given the intrinsic luminosity function and N_c is the number of objects which would potentially contaminate the luminosity function. The corresponding values for the observed sample are n_z and n_c where the total number of objects in the galaxy sample is given by $n_t = n_z + n_c$. If \mathcal{C} individual fields are included in the sample this is accounted for by taking the product over the \mathcal{C} fields where c_l corresponds to the number of objects in the l 'th field such that $n_t = \sum_l^{\mathcal{C}} c_l$. The ratio A_l/A_{sky} gives the fractional area the l 'th field covers on the sky. The C_b^a terms are binomial coefficients which can be expressed in terms of the logarithm of the gamma function as

$$\ln(C_b^a) = \ln \Gamma(a+1) - \ln \Gamma(b+1) - \ln \Gamma(a-b+1). \quad (\text{C9})$$

The number of contaminants is determined by the contamination fraction f . By approximating the number of contaminants by its expectation value such that

$$N_c = \frac{f}{1-f} N_z \quad c_{lc} = \frac{f}{1-f} c_{lz} \quad n_c = f n_t \quad n_z = (1-f) n_t$$

Equation (C8) becomes

$$p(\theta \mid L_{J,\text{obs}}, I_V = 0) \propto p(\theta) C_{(1-f)n_t}^{N_z} C_{f n_t}^{\frac{f}{1-f} N_z} \prod_l^{\mathcal{C}} [1 - A_l/A_{\text{sky}} p(I=1|\theta)]^{\frac{1}{1-f_l} (N_z - (1-f_l) c_l)} \times \prod_i^{n_t} p(L_{J,\text{obs},i}|\theta) \quad (\text{C10})$$

Here the contamination f varies between each field contributing to the final sample as indicated by the subscript l . The $p(I=1|\theta)$ term on the right-hand-side represents the probability distribution of an object making it into the sample but is independent on the individual observations. However, it differs between the different observed fields (or surveys) in the sample as exposure times and hence depths differ from field to field. Expanding the detection probability for the considered sample we have that

$$p(I=1|\theta) = \int_0^\infty p(I=1|L_{J,\text{obs}}) p(L_{J,\text{obs}}|\theta) dL_{J,\text{obs}}. \quad (\text{C11})$$

Here $p(I=1|L_{J,\text{obs}})$ is the selection function for the l 'th field accounted for completeness.

The last term on the right-hand-side in Equation (C10) also appearing in Equation (C11) represents the likelihood of the i 'th object in the sample which can be expressed as

$$\begin{aligned} p(L_{J,\text{obs}}|\theta) &= \int_0^\infty p(L_{J,\text{obs}}|L_{J,\text{true}}) p(L_{J,\text{true}}|\theta) dL_{J,\text{true}} \\ &\propto \int_0^\infty \mathcal{N}(L_{J,\text{obs}}|L_{J,\text{true}}, \delta L_{J,\text{field}}) \text{gamma}(L_{J,\text{true}}|k, L^*) dL_{J,\text{true}}. \end{aligned} \quad (\text{C12})$$

Where we use $p(L) \propto \frac{\Phi(L)}{\phi^*}$ (see Equation (1) of Kelly et al. 2008) and that $\text{gamma}(L_{J,\text{true}}|k, L^*)$ is related to the Schechter luminosity function $\Phi(L_{J,\text{true}})$ as shown in Equation (C2).

$$\mathcal{N}(L_{J,\text{obs}}|L_{J,\text{true}}, \delta L_{J,\text{field}}) = \frac{1}{\delta L_{J,\text{field}} \sqrt{2\pi}} \exp\left(-\frac{(L_{J,\text{true}} - L_{J,\text{obs}})^2}{2 \delta L_{J,\text{field}}^2}\right) \quad (\text{C13})$$

represents the true luminosity inferred from the observations assuming a Gaussian measurement error with $\delta L_{J,\text{field}}$ being the median photometric error in the J-band in the given field.

By denoting the selection function with $\mathcal{S}(L_{J,\text{obs}})$ and defining

$$\mathcal{F}(L_{J,\text{true}}) = \mathcal{N}(L_{J,\text{obs}}|L_{J,\text{true}}, \delta L_{J,\text{field}}) \text{gamma}(L_{J,\text{true}}|k, L^*) \quad (\text{C14})$$

we can express Equation (C10) as

$$\begin{aligned} p(\theta \mid L_{J,\text{obs}}, I_V = 0) &\propto p(\theta) \\ &\times C_{(1-f)n_t}^{N_z} C_{f n_t}^{\frac{f}{1-f} N_z} \prod_l^{\mathcal{C}} \left[1 - A_l/A_{\text{sky}} \int_0^\infty \mathcal{S}(L_{J,\text{obs}}) \int_0^\infty \mathcal{F}(L_{J,\text{true}}) dL_{J,\text{true}} dL_{J,\text{obs}} \right]^{\frac{1}{1-f_l} (N_z - (1-f_l) c_l)} \\ &\times \prod_i^{n_t} \int_0^\infty \mathcal{F}(L_{J,\text{true}}) dL_{J,\text{true}} \end{aligned} \quad (\text{C15})$$

This is the posterior probability distribution for a sample of n_t objects assumed to be binomially distributed and to have an intrinsic Schechter luminosity function on the form shown in Equation (C1), where each observed luminosity is related to the true luminosity through an assumed Gaussian error distribution and where the prior on $\log_{10} N_z$ is uniform.

Estimating $p(\theta \mid L_{J,\text{obs}}, I_V = 0)$ for a certain θ corresponds to estimating the probability that the luminosity function with the parameters (k, L^*, N_z) is the intrinsic luminosity function of the analyzed galaxy sample. The

intrinsic luminosity function can for instance be obtained from this expression by sampling θ via a Markov Chain Monte Carlo approach. As described in Section 4 we used such an approach to infer the intrinsic luminosity function at redshift 8 for the BoRG13 sample.

Having obtained the three-dimensional posterior distribution for θ the number density of high redshift galaxies, ϕ^* , and the luminosity density, ϵ , can be determined using Equations (C4) and (C6). The current framework assumes that the fraction of contaminants is independent of luminosity for the BoRG sample.

Above we have partially followed Kelly et al. (2008) and refer to this work for further details.

REFERENCES

- Baker, J. G., & Menzel, D. H. 1938, *Astrophysical Journal*, 88, 52
- Benítez, N., Ford, H., Bouwens, R., et al. 2004, *The Astrophysical Journal Supplement Series*, 150, 1
- Bertin, E., & Arnouts, S. 1996, *Astronomy and Astrophysics Supplement*, 117, 393
- Bolton, J. S., & Haehnelt, M. G. 2013, *Monthly Notices of the Royal Astronomical Society*, 429, 1695
- Bouwens, R. J., Illingworth, G. D., Blakeslee, J. P., Broadhurst, T. J., & Franx, M. 2004, *The Astrophysical Journal*, 611, L1
- Bouwens, R. J., Illingworth, G. D., Blakeslee, J. P., & Franx, M. 2006, *The Astrophysical Journal*, 653, 53
- Bouwens, R. J., Illingworth, G. D., Franx, M., & Ford, H. 2007, *The Astrophysical Journal*, 670, 928
- Bouwens, R. J., Illingworth, G. D., Oesch, P. A., et al. 2010, *The Astrophysical Journal Letters*, 709, L133
- . 2011, *The Astrophysical Journal*, 737, 90
- . 2012, *The Astrophysical Journal Letters*, 752, L5
- Bradley, L. D., Trenti, M., Oesch, P. A., et al. 2012, *The Astrophysical Journal*, 760, 108
- Bradley, L. D., Zitrin, A., Coe, D., et al. 2013, eprint arXiv, 1308, 1692
- Cai, Z.-Y., Lapi, A., Bressan, A., et al. 2014, eprint arXiv, 1403, 55
- Capak, P., Faisst, A., Vieira, J. D., et al. 2013, *The Astrophysical Journal Letters*, 773, L14, accepted to ApJL, 5 Pages, 4 Figures, 1 Table
- Cara, M., & Lister, M. L. 2008, *The Astrophysical Journal*, 686, 148
- Cardelli, J. A., Clayton, G. C., & Mathis, J. S. 1989, *Astrophysical Journal*, 345, 245
- Caruana, J., Bunker, A. J., Wilkins, S. M., et al. 2012, *Monthly Notices RAS*, 427, 3055
- . 2013, eprint arXiv, 1311, 57, submitted to MNRAS
- Casertano, S., de Mello, D., Dickinson, M., et al. 2000, *The Astronomical Journal*, 120, 2747
- Coe, D., Benítez, N., Sánchez, S. F., et al. 2006, *The Astronomical Journal*, 132, 926
- Dijkstra, M., Mesinger, A., & Wyithe, J. S. B. 2011, *Monthly Notices of the Royal Astronomical Society*, 414, 2139
- Dunlop, J. S. 2013, *The First Galaxies*, 396, 223
- Dunlop, J. S., McLure, R. J., Robertson, B. E., et al. 2012a, *Monthly Notices RAS*, 420, 901
- Dunlop, J. S., Rogers, A. B., McLure, R. J., et al. 2012b, eprint arXiv, 1212, 860, 13 pages, 7 figures, submitted to MNRAS
- Ellis, R. S., McLure, R. J., Dunlop, J. S., et al. 2012, eprint arXiv, 1211, 6804
- Faisst, A. L., Capak, P., Carollo, C. M., Scarlata, C., & Scoville, N. 2014, eprint arXiv, 1402, 3604, 11 pages, 6 figures, 2 tables, submitted to ApJ
- Ferguson, H. C., Dickinson, M., Giavalisco, M., et al. 2004, *The Astrophysical Journal*, 600, L107
- Fernandez, E. R., & Shull, J. M. 2011, *The Astrophysical Journal*, 731, 20
- Finkelstein, S. L., Papovich, C., Giavalisco, M., et al. 2010, *The Astrophysical Journal*, 719, 1250
- Finkelstein, S. L., Papovich, C., Salmon, B., et al. 2012, *The Astrophysical Journal*, 756, 164
- Finkelstein, S. L., Papovich, C., Dickinson, M., et al. 2013, eprint arXiv, 1310, 6031
- Finlator, K., Oh, S. P., Özel, F., & Davé, R. 2012, *Monthly Notices of the Royal Astronomical Society*, 427, 2464
- Fontana, A., Vanzella, E., Pentericci, L., et al. 2010, *The Astrophysical Journal Letters*, 725, L205
- Grogin, N. A., Kocevski, D. D., Faber, S. M., et al. 2011, *The Astrophysical Journal Supplement*, 197, 35
- Illingworth, G. D., Magee, D., Oesch, P. A., et al. 2013, eprint arXiv, 1305, 1931
- Jaacks, J., Thompson, R., & Nagamine, K. 2013, eprint arXiv, 1301, 5270, 6 pages, 4 figures, submitted
- Kaurov, A. A., & Gnedin, N. Y. 2013, eprint arXiv, 1311, 2594, 6 pages, 5 figures, submitted to ApJ
- Kelly, B. C., Fan, X., & Vestergaard, M. 2008, *The Astrophysical Journal*, 682, 874
- Koekemoer, A. M., Fruchter, A. S., Hook, R. N., & Hack, W. 2003, *The 2002 HST Calibration Workshop : Hubble after the Installation of the ACS and the NICMOS Cooling System*, 337
- Koekemoer, A. M., Faber, S. M., Ferguson, H. C., et al. 2011, *The Astrophysical Journal Supplement*, 197, 36
- Koekemoer, A. M., Ellis, R. S., McLure, R. J., et al. 2012, eprint arXiv, 1212, 1448, 16 pages, 9 figures, submitted to ApJS
- Lorenzoni, S., Bunker, A. J., Wilkins, S. M., et al. 2011, *Monthly Notices RAS*, 414, 1455
- Madau, P., Ferguson, H. C., Dickinson, M. E., et al. 1996, *Monthly Notices RAS*, 283, 1388
- McLure, R. J., Dunlop, J. S., Cirasuolo, M., et al. 2010, *Monthly Notices of the Royal Astronomical Society*, 403, 960
- McLure, R. J., Dunlop, J. S., Bowler, R. A. A., et al. 2013, *Monthly Notices of the Royal Astronomical Society*, 432, 2696, 19 pages, 7 figures, submitted to MNRAS
- McQuinn, M., Oh, S. P., & Faucher-Giguère, C.-A. 2011, *The Astrophysical Journal*, 743, 82
- Oesch, P. A., Stiavelli, M., Carollo, C. M., et al. 2007, *The Astrophysical Journal*, 671, 1212
- Oesch, P. A., Carollo, C. M., Stiavelli, M., et al. 2009, *The Astrophysical Journal*, 690, 1350
- Oesch, P. A., Bouwens, R. J., Carollo, C. M., et al. 2010a, *The Astrophysical Journal Letters*, 725, L150
- . 2010b, *The Astrophysical Journal Letters*, 709, L21
- Oesch, P. A., Bouwens, R. J., Illingworth, G. D., et al. 2010c, *The Astrophysical Journal Letters*, 709, L16
- . 2012, *The Astrophysical Journal*, 759, 135
- . 2013, *The Astrophysical Journal*, 773, 75, 21 pages, 13 figures, 6 tables; submitted to ApJ
- Ono, Y., Ouchi, M., Curtis-Lake, E., et al. 2012a, eprint arXiv, 1212, 3869, 15 pages, 13 figures, submitted to ApJ
- Ono, Y., Ouchi, M., Mobasher, B., et al. 2012b, *The Astrophysical Journal*, 744, 83
- Ouchi, M., Mobasher, B., Shimasaku, K., et al. 2009, *The Astrophysical Journal*, 706, 1136
- Ouchi, M., Shimasaku, K., Furusawa, H., et al. 2010, *The Astrophysical Journal*, 723, 869
- Reddy, N. A., & Steidel, C. C. 2009, *The Astrophysical Journal*, 692, 778
- Robertson, B. E., Furlanetto, S. R., Schneider, E., et al. 2013, *The Astrophysical Journal*, 768, 71
- Schechter, P. 1976, *Astrophysical Journal*, 203, 297, a&AA ID. AAA017.158.009
- Schenker, M. A., Robertson, B. E., Ellis, R. S., et al. 2013, *The Astrophysical Journal*, 768, 196, 15 pages, 5 figures, To be submitted to ApJ
- Shull, J. M., Harness, A., Trenti, M., & Smith, B. D. 2012, *The Astrophysical Journal*, 747, 100
- Stark, D. P., Ellis, R. S., Chiu, K., Ouchi, M., & Bunker, A. 2010, *Monthly Notices RAS*, 408, 1628
- Stark, D. P., Schenker, M. A., Ellis, R., et al. 2013, *The Astrophysical Journal*, 763, 129
- Steidel, C. C., Adelberger, K. L., Shapley, A. E., et al. 2000, *The Astrophysical Journal*, 532, 170

- Steidel, C. C., Giavalisco, M., Pettini, M., Dickinson, M., & Adelberger, K. L. 1996, *Astrophysical Journal Letters* v.462, 462, L17
- Tacchella, S., Trenti, M., & Carollo, C. M. 2013, *The Astrophysical Journal Letters*, 768, L37
- Tanvir, N. R., Levan, A. J., Fruchter, A. S., et al. 2012, *The Astrophysical Journal*, 754, 46
- Trenti, M., Perna, R., Levesque, E. M., Shull, J. M., & Stocke, J. T. 2012a, *The Astrophysical Journal Letters*, 749, L38
- Trenti, M., & Stiavelli, M. 2008, *The Astrophysical Journal*, 676, 767
- Trenti, M., Stiavelli, M., Bouwens, R. J., et al. 2010, *The Astrophysical Journal Letters*, 714, L202
- Trenti, M., Bradley, L. D., Stiavelli, M., et al. 2011, *The Astrophysical Journal Letters*, 727, L39
- . 2012b, *The Astrophysical Journal*, 746, 55
- Treu, T., Schmidt, K. B., Trenti, M., Bradley, L. D., & Stiavelli, M. 2013, *The Astrophysical Journal Letters*, 775, L29
- Treu, T., Trenti, M., Stiavelli, M., Auger, M. W., & Bradley, L. D. 2012, *The Astrophysical Journal*, 747, 27
- van Dokkum, P. G. 2001, *The Publications of the Astronomical Society of the Pacific*, 113, 1420
- Vanzella, E., Giavalisco, M., Dickinson, M., et al. 2009, *The Astrophysical Journal*, 695, 1163
- Vihola, M. 2012, *Statistics and Computing*
- Yan, H., Yan, L., Zamojski, M. A., et al. 2011, *The Astrophysical Journal Letters*, 728, L22
- Yuan, Z., & Wang, J. 2013, eprint arXiv, 1302, 5887
- Zaroubi, S. 2013, *The First Galaxies*, 396, 45